PNC TN9410 93-203

A Study of Traveling Wave Resonant Ring Characteristics

March, 1993

OARAI ENGINEERING CENTER
POWER REACTOR AND NUCLEAR FUEL DEVELOPMENT CORPORATION

複製又はこの資料の入手については，下記にお問い合わせください。
〒311-13　茨城県東茨城郡大洗町成田町4002
動力炉・核燃料開発事業団
大洗工学センター　システム開発推進部・技術管理室

Enquires about copyright and reproduction should be addressed to: Technology Management Section O-arai Engineering Center, Power Reactor and Nuclear Fuel Development Corporation 4002 Narita-cho, O-arai-machi, Higashi-Ibaraki, Ibaraki-ken, 311-13, Japan

動力炉・核燃料開発事業団（Power Reactor and Nuclear Fuel Development Corporation）

PNC TN9410 93-203
MARCH 1993

Wang Yualin*

Abstract

The characteristics of TWRR are analysed in detail. They include effects of the reflection, coupling coefficient and directivity. The characteristics of TWRR with an accelerator section are studied. They include analyses of constant impedance structure, with fixed coupling and optimal coupling, and on/off beam loading. The characteristics of constant gradient structure are also analysed. Q values of TWRR and TWRR with an accelerator section are calculated.

TWRRs with RF window and with an accelerator section are tested in low power and high power. Some phenomena appeared are mentioned and analysed. The stability of TWRR with an accelerator section is discussed.

The results of tests show that the measured parameters of TWRR with an accelerator section are in very good agreement with the calculated values.

* Guest Reseacher of PNC (Nanjing University)

PNC TN9410 93-203
１９９３年３月

進行波還流型レゾナントリングの特性に関する研究

王　元林*

要　旨

進行波還流型レゾナントリング（ＴＷＲＲ）の特性について、解析と試験の結果を比較評価した。

還流部の特性解析では、マイクロ波（ＲＦ）の反射、結合係数、方向性の効果を考慮した。加速管部の解析では、一定インピーダンス型と電場一定型構造の加速管についてＲＦ特性を解析し、ビームローデングのある場合とない場合の比較評価を行った。また、結合係数一定の場合と電流値の変化に合わせて最適な結合係数になるように設定した場合の比較も行った。Ｑ値については、還流部のみの場合と加速管部も含めた総合的なものについても求めた。

試作したＴＷＲＲを用いて、低出力と高出力のＲＦ試験を行った。試験の結果をもとに、ＴＷＲＲの安定性について解析評価した。また、同様にＴＷＲＲを用いて、クライストロンの窓部（ＲＦ窓）単体の特性についても評価した。

その結果、特性解析の結果と試験結果は、良く一致することが確認された。

＊大洗工学センター技術開発部先進技術開発室客員研究員（南京大学助教授）

Contents

List of Tables

List of Figures

1, Introduction

The traveling wave resonant ring (TWRR) is an interesting microwave circuit. Not only it has most advantages of the standing wave resonant cavity (SWRC), such as a high Q value and high RF field, but also some unique characteristics as follows.

First one is that the RF field in TWRR is added by fields transmitted in the same direction, while the field in SWRC is added by fields transmitted in the opposite direction. Therefore, with the linear accelerator using TWRR, one can get a pure traveling wave to accelerate electrons efficiently, In contrast, that using SWRC, only one directional fields can contribute to accelerating electrons.

Second one is a good frequency characteristic, as shown in Fig.1 where frequency characteristics of SWRC and TWRR are compared.

In regard to SWRC, Fig.1 (a) indicates that, as far as a cavity is under the optimal coupling condition at resonant frequency, no power reflection occurs. But once the frequency deviation occurs from its resonant condition, most input power into SWRC is reflected by the cavity.

For TWRR, under the optimal coupling condition, at the resonant frequency there is no power reflected and no power passes through to the dummy load, when the frequency deviating resonant frequency most input power passes through to the dummy load and there is no power reflected yet. It is important to protect RF source against reflection. Figure 1 (b) shows its characteristic.

Now let us discuss TWRR.

2, Steady state

2-1, A simple TWRR

For a simple TWRR shown in Fig.2, a waveguide ring is coupled with a main transmission line through a directional coupler. A wave progressing from the signal source to port 1 is partially coupled into the ring at port 4 and circulates around the ring in the direction indicated. When this wave passes the port 3 in the coupling region, a fraction is coupled into the port 2 (dummy load) with the remainder circulating around the ring again. At the same time, more energy is coupled from the main line into the ring. If the wave circulating around the ring and the wave coupled into the ring are in phase at the coupled section, the wave in the ring can be build up and becomes quite large in its magnitude.

The above discussion shows three factors to be considered in a practical resonant ring. First, the length, L, of the ring must be such that the waves will be in phase. This means that the length of the ring (phase) or the frequency of the source or both must be variable to make the ring at resonance. Second, the coupling with the ring should be chosen near its optimal coupling to compensate for losses. Third, some method is needed to cancel out any backward wave in the ring to make the ring matching.

Such characteristics of this circuit can be expressed as follows. Assuming that a_1, a_2, a_3 and a_4 are input waves on the port 1, port 2, port 3 and port 4 of the directional coupler respectively and b_1, b_2, b_3 and b_4 are output waves respectively. E_0 is input signal and suppose that there is no reflection in the ring, the dummy load is ideal i.e. no reflection and the directional coupler is ideal one with infinite directivity, one can list the following a set of equations:

$$
\begin{cases}
a_1 = E_0 \\
a_2 = 0 \\
a_3 = b_4 T\, e^{-j\varphi} \\
a_4 = 0 \\
b_1 = a_2 \sqrt{1-C^2}\, e^{-j\psi_2} + a_4 C\, e^{-j\psi_1} \\
b_2 = a_1 \sqrt{1-C^2}\, e^{-j\psi_2} + a_3 C\, e^{-j\psi_1} \\
b_3 = a_2 C\, e^{-j\psi_1} + a_4 \sqrt{1-C^2}\, e^{-j\psi_2} \\
b_4 = a_1 C\, e^{-j\psi_1} + a_3 \sqrt{1-C^2}\, e^{-j\psi_2}
\end{cases}
\qquad (1)
$$

Where T is voltage transmission coefficient of the ring,

$$T = e^{-\tau_w} \tag{2}$$

τ_w is the attenuation constant $\tau_w = \alpha_w L_w$, where α_w is attenuation in nepers per unit length and L_w the length of the waveguide in the ring.

Where φ is the total phase of the ring,

$$\varphi = \beta_w L_w \tag{3}$$

β_w is phase constant of the waveguide.

The directional coupler has a coupling coefficient $C\ e^{-j\psi_1}$ and a transmission coefficient of $\sqrt{(1-C^2)}\ e^{-j\psi_2}$, where $\psi 1 - \psi 2 = \pm \pi/2$.

The multiplication factor M is defined by Eq.(4)

$$M = \frac{b_4}{a_1} = \frac{C\ e^{-j\psi_1}}{1 - T\sqrt{1-C^2}\ e^{-j(\varphi+\psi_2)}} \tag{4}$$

The nullification factor N is defined by Eq.(5)

$$N = \frac{b_2}{a_1} = \sqrt{1-C^2}\,e^{-j\psi_2} - \frac{C^2\ T\ e^{-j(\varphi+2\psi_1)}}{1 - T\sqrt{1-C^2}\,e^{-j(\varphi+\psi_2)}} \tag{5}$$

Usually, assuming $\psi_2 = 0$, so $\psi_1 = \pi/2$, Eqs.(4) and (5) become following:

$$M = \frac{jC}{1 - T\sqrt{1-C^2}\ e^{-j\varphi}} \tag{6}$$

$$N = \sqrt{1-C^2} - \frac{C^2\ T\ e^{-j\varphi}}{1 - T\sqrt{1-C^2}\ e^{-j\varphi}} \tag{7}$$

The module $|M|$ and argument θ of the M are given by:

$$|M| = \frac{C}{\sqrt{1 + T^2(1-C^2) - 2T\sqrt{1-C^2}\cos\varphi}} \quad (8)$$

$$\theta = \arg(M) = \frac{\pi}{2} - \arctan\left(\frac{-T\sqrt{1-C^2}\sin\varphi}{1 - T\sqrt{1-C^2}\cos\varphi}\right) \quad (9)$$

The module $|N|$ and argument Ψ of N are given by:

$$|N| = \sqrt{T^2C^2M^2 + (1-C^2) - 2TCM\cos(\varphi+\theta+\pi/2)} \quad (10)$$

$$\Psi = \arg(N) = \arctan\left(\frac{TCM\sin(\varphi+\theta-\pi/2)}{\sqrt{1-C^2} - TCM\cos(\varphi+\theta-\pi/2)}\right) \quad (11)$$

The module $|M|$ and arguments θ vs. φ and module $|N|$ and argument Ψ vs. φ for a given C=0.2939 and T=0.9438 values are showed on Fig.3 and Fig.4, respectively.

At resonance, i.e. the phase of the ring is equal to $2n\pi$, M and N become their maximum and minimum respectively, therefore, Eqs.(6) and (7) become

$$M = \frac{C}{1 - T\sqrt{1-C^2}} \quad (12)$$

$$N = \sqrt{1-C^2} - \frac{C^2T}{1 - T\sqrt{1-C^2}} \quad (13)$$

M and N vs. C for given T values are shown on the Fig.5 and Fig 6, respectively.

At the optimal coupling i.e. at $C = \sqrt{(1-T^2)}$, M of Eq.(12) becomes its maximum,

$$M = \frac{1}{\sqrt{1-T^2}} = \frac{1}{C} \qquad (14)$$

and Eq. (13) becomes zero

$$N = 0 \qquad (15)$$

Eq.(14) is indicated by a dashed line in the Fig.5 and where no power is transmitted to the dummy load.

Above analyses show that the maximal efficiency of TWRR is at resonance with optimal coupling conditions. Design and operation of a ring at these conditions are desirable.

For TWRR, in order to make it resonance changing the frequency of RF source is convenient, but for some case it is impossible. In that case, for a given frequency a phase shifter in the ring is necessary to tune TWRR at resonance.

If the main coupler has a fixed coupling coefficient, the TWRR can be operated with only one point at its optimal efficiency. If one want to operate at optimal efficiency in some region, a coupler having a variable coupling coefficient is needed.

2-1-1, The simple TWRR with some reflection

Now let us analyze the ring in which there is some reflection having a reflection coefficient of $\Gamma\, e^{-j\theta_1}$ and a transmission coefficient of $\sqrt{(1-\Gamma^2)}\, e^{-j\theta_2}$, where $\theta_1 - \theta_2 = \pm\pi/2$, Eq.(1) can be rewritten as following:

$$\begin{cases} a_1 = E_0 \\ a_2 = 0 \\ a_3 = b_3 T_2 e^{-j\varphi_2} \Gamma\, e^{-j\theta_1} T_2 e^{-j\varphi_2} + b_4 T_1 e^{-j\varphi_1} \sqrt{1-\Gamma^2}\, e^{-j\theta_2} T_2 e^{-j\varphi_2} \\ a_4 = b_3 T_2 e^{-j\varphi_2} \sqrt{1-\Gamma^2}\, e^{-j\theta_2} T_1 e^{-j\varphi_1} + b_4 T_1 e^{-j\varphi_1} \Gamma\, e^{-j\theta_1} T_1 e^{-j\varphi_1} \\ b_1 = a_2 \sqrt{1-C^2}\, e^{-j\psi_2} + a_4 C\, e^{-j\psi_1} \\ b_2 = a_1 \sqrt{1-C^2}\, e^{-j\psi_2} + a_3 C\, e^{-j\psi_1} \\ b_3 = a_2 C\, e^{-j\psi_1} + a_4 \sqrt{1-C^2}\, e^{-j\psi_2} \\ b_4 = a_1 C\, e^{-j\psi_1} + a_3 \sqrt{1-C^2}\, e^{-j\psi_2} \end{cases} \qquad (16)$$

From eq.(16) we can get solutions:

$$M = \frac{C\,e^{-j\psi_1} - C\,T\sqrt{1-C^2}\sqrt{1-\Gamma^2}\,e^{-j(\varphi+\theta_2+\psi_1+\psi_2)}}{1-2\,T\sqrt{1-C^2}\sqrt{1-\Gamma^2}\,e^{-j(\varphi+\theta_2+\psi_2)} + T^2(1-C^2)\,e^{-j(2\varphi+2\psi_2)}} \qquad (17)$$

$$\Gamma_1 = \frac{b_1}{a_1} = \frac{-C^2\,T_1^2\,\Gamma\,e^{-j(2\varphi_1+\theta_1+2\psi_1)}}{1-2\,T\sqrt{1-C^2}\sqrt{1-\Gamma^2}\,e^{-j(\varphi+\theta_2+\psi_2)} + T^2(1-C^2)\,e^{-j(2\varphi+2\psi_2)}} \qquad (18)$$

$$\Gamma_4 = \frac{a_4}{b_4} = \frac{T_1^2\,\Gamma e^{-j(2\varphi_1+\theta_1)}}{1-T\sqrt{1-C^2}\sqrt{1-\Gamma^2}\,e^{-j(\varphi+\theta_2+\psi_2)}} \qquad (19)$$

$$N = \frac{\sqrt{1-C^2}\,e^{-j\psi_2}\,(1-T^2e^{-j2\varphi}) - T\sqrt{1-\Gamma^2}\,e^{-j(\varphi+\theta_2)}\,(2+C^2e^{-j2\varphi_1})}{1-2\,T\sqrt{1-C^2}\sqrt{1-\Gamma^2}\,e^{-j(\varphi+\theta_2+\psi_2)} + T^2(1-C^2)\,e^{-j(2\varphi+2\psi_2)}} \qquad (20)$$

Figures 7 and 8 are 3-dimensions graphs of module M and argument θ vs.φ and Γ for T=0.9438 and C=0.2939, respectively.

Figures 9 and 10 are 3-dimensions graphs of module N and argument ψ vs.φ and Γ for T=0.9438 and C=0.2939, respectively.

Figures 11 and 12 are 3-dimensions graphs of module Γ_1 and module Γ_4 vs.φ and Γ for T=0.9438 and C=0.2939, respectively.

These results show that if there is some reflection in TWRR, the multiplication factor M will go down, the power to the load will go up and the reflection in the ring and at input port will become very large. All of them are not desirous. Therefore, it is important to cancel the reflection in TWRR using a impedance matcher (for example, a stub tuner).

2-1-2, Effect of directivity of the coupler

In the 2-1-1 section the directional coupler is considered to be ideal, i.e. it is a coupler with infinite directivity. Now one will discuss about it in the real case. Let us suppose that the directional coupler have

$$\frac{b_4}{a_1} = C\ e^{-j\psi_1}\sqrt{1-D^2}\ e^{-j\eta_2}$$

$$\frac{b_2}{a_1} = \sqrt{1-C^2}\ e^{-j\psi_2} \tag{21}$$

$$\frac{b_3}{a_1} = C\ e^{-j\psi_1}\ D\ e^{-j\eta_1}$$

where C is the voltage coupling coefficient, D the directivity and $\eta_1-\eta_2=\pm\pi/2$.

Equation (1) becomes following:

$$\begin{cases} a_1 = E_0 \\ a_2 = 0 \\ a_3 = b_4 T\ e^{-j\varphi} \\ a_4 = b_3 T\ e^{-j\varphi} \\ b_1 = a_3 C\ e^{-j\psi_1} D\ e^{-j\eta_1} + a_4\ C\ e^{-j\psi_1}\sqrt{1-D^2}\ e^{-j\eta_2} \\ b_2 = a_1\sqrt{1-C^2}\ e^{-j\psi_2} + a_3\ C\ e^{-j\psi_1}\sqrt{1-D^2}\ e^{-j\eta_2} + a_4 C e^{-j\psi_1} D e^{-j\eta_1} \\ b_3 = a_1\ C\ e^{-j\psi_1} D\ e^{-j\eta_1} + a_4\ \sqrt{1-C^2}\ e^{-j\psi_2} \\ b_4 = a_1\ C\ e^{-j\psi_1}\sqrt{1-D^2}\ e^{-j\eta_2} + a_3\ \sqrt{1-C^2}\ e^{-j\psi_2} \end{cases} \tag{22}$$

Its solutions are:

$$M = \frac{C\sqrt{1-D^2}\ e^{-j(\psi_1+\eta_2)}}{1 - T\sqrt{1-C^2}\ e^{-j(\varphi+\psi_2)}} \tag{23}$$

$$\Gamma_1 = \frac{2C^2 D T\sqrt{1-D^2}\ e^{-j(2\psi_1+\eta_1+\eta_2+\varphi)}}{1 - T\sqrt{1-C^2}\ e^{-j(\varphi+\psi_2)}} \tag{24}$$

$$\Gamma_4 = \frac{DT\ e^{-j(\eta_1+\varphi)}}{\sqrt{1-D^2}\ e^{-j\eta_2}} \tag{25}$$

$$N = \sqrt{1-C^2}\ e^{-j\psi_2} + \frac{C^2 T\ e^{-j(2\psi_1+\varphi)}}{1 - T\sqrt{1-C^2}\ e^{-j(\varphi+\psi_2)}} \tag{26}$$

When TWRR at resonance and under optimal coupling condition the equations (23),(24),(25) and (26) become following

$$M = \frac{C\sqrt{1-D^2}}{1-T\sqrt{1-C^2}} \tag{27}$$

$$\Gamma_1 = 2DT\sqrt{1-D^2} \tag{28}$$

$$\Gamma_4 = \frac{2DT}{\sqrt{1-D^2}} \tag{29}$$

$$N = 0 \tag{30}$$

From above results one can estimate what directivity will be required. For example, for a TWRR transmission coefficient T=0.9438, and coupling coefficient C=0.55, table 1 lists calculated data.

Table 1, Effect of the directivity

Directivity	(D)	T	C	M	Γ_1	Γ_4
20 db	0.100	0.9438	0.550	2.584	0.268	0.085
25 db	0.0562	0.9438	0.550	2.592	0.151	0.053
28 db	0.0398	0.9438	0.550	2.594	0.107	0.037
30 db	0.0316	0.9438	0.550	2.596	0.085	0.030

If we want to keep $\Gamma_1 < 0.1$ we must require directivity higher than 28dB. In this case the directivity has not so large influence on the multiplication factor M.

2-1-3, The simple TWRR Q value

According to the resonant curve of TWRR, the Q_L of the simple TWRR can be derived as following

$$Q_L = \frac{f}{2\Delta f} = \frac{\varphi_w \left(\frac{\lambda_g}{\lambda_0}\right)^2}{2\arccos\left(\frac{4T\sqrt{1-C^2} - T^2(1-C^2)-1}{2T\sqrt{1-C^2}}\right)} \qquad (31)$$

where λ_0 and λ_g are wavelength of the free space and waveguide, respectively.

For the same total phase and different T, the curves of Q vs. C are shown on the Fig.13 (a). When C=0, the Q values are Q_0. Under the optimal coupling, the loaded Q_L values are equal to $Q_0/2$.

2-1-4, Applications of the simple TWRR

The most applications of TWRR are high power simulation for microwave transmission components under a pure traveling wave.

For example, an RF window test system is shown on Fig.14. A test Rf window inserts in the ring, and there is a stub tuner for matching the ring and a phase shifter for tuning the ring at resonance.

If the attenuation in the whole ring is very low, the multiplication factor will be very high. For example, T=0.9972,and C=0.2939, one can get M=6.33. So the power gain is about 40, this means that if input power is 50KW, the test power in the ring is 2MW that power is very difficult to get from the klystron in CW operation.

2-2, A TWRR with an accelerator section

2-2-1, Accelerator without beam loading

Fig.15 shows the TWRR with an accelerator section. Let us suppose that the attenuation and phase of the accelerator section be τ_a and φ_a respectively, and ones of the waveguide components in the TWRR be τ_w and φ_w respectively. The transmission coefficient T and φ phase of the total resonant ring include two parts. Eqs.(2) and (3) become following

$$T = e^{-\tau_w} \; e^{-\tau_a} \tag{32}$$

$$\varphi = \varphi_w + \varphi_a \tag{33}$$

Substitution of Eqs.(32) and (33) into Eqs. from (4) to (30) gives the multiplication factor M and nullification factor N for various cases, respectively. For example, the table 2 lists the attenuations of our accelerator and TWRR waveguide parts and calculated M at resonant point for fixed coupling coefficient (C=0.2939).

Table 2, Multiplication of TWRR
(for given coupling coefficient C=0.2939)

	τ_{all}				τ_{all}	T	M
	τ_a	τ_w					
		τ_{ps}	τ_{st}	τ_{ow}			
design value	0.0534	0.00115	0.00115	0.0021	0.0575	0.9438	3.00
actual value							
case 1	0.0536	0.01610	0.00072	0.0020	0.0724	0.9302	2.65
case 2	0.0536	0.00774	0.00072	0.0020	0.0641	0.9379	2.84
case 3	0.0536	———	0.00072	0.0026	0.0569	0.9447	3.03

where τ_a, τ_w and τ_{all} are attenuation of accelerator, waveguide of resonant ring and total of resonant ring, respectively.

$\tau_w = \tau_{ps} + \tau_{st} + \tau_{ow}$, where τ_{ps}, τ_{st} and τ_{ow} are attenuation of the phase shifter, stub tuner and other waveguide in the resonant ring, respectively.

For the actual case 1, the attenuation of the phase shifter was very large; for the case 2, after the phase shifter improved the attenuation was little bit low; and for the case 3, there is no phase shifter in the resonant ring so the multiplication factor is slightly higher than the design value.

Fig.3 and Fig.4 show the multiplication factor M and nullification factor N of the TWRR with Accelerator section without beam loading according to the design data. Near the resonant point the changing rate of the phase is very large.

$$\frac{d\theta}{d\varphi} = 9.22 \qquad \frac{d\psi}{d\varphi} = 68.71$$

2-2-2, Accelerator section with beam loading

(1), For constant impedance structure

For the constant impedance accelerator structure, its shunt impedance R and attenuation α_a are constants, so the attenuation constant $\tau_a = \alpha_a L_a$, where L_a is length of accelerator section. τ_w is the attenuation constant of waveguide in the resonant ring, $\tau = \tau_a + \tau_w$, P is input power, $E = \sqrt{(2 P \alpha_a R)}$ is electric field and I is beam current. We can get multiplication factor M from following formulae:

a), for fixed coupling coefficient C

$$M = \frac{C - \frac{IR}{E}\sqrt{1-C^2}\,(1-e^{-\tau_a})\,e^{-\tau_w}}{1-\sqrt{1-C^2}\,e^{-\tau}} \qquad (34)$$

When the attenuation of the waveguide components can be

neglected as compared with one of the accelerator, eq.(34) becomes

$$M = \frac{C - \frac{IR}{E}\sqrt{1-C^2}\,(1-e^{-\tau_a})}{1-\sqrt{1-C^2}\,e^{-\tau_a}} \tag{35}$$

b), for optimal coupling coefficient C =1/M

$$M = \frac{\sqrt{\frac{I^2R^2}{E^2}(1-e^{-\tau_a})^2 e^{-2\tau_w} + (1-e^{-2\tau})} - \frac{IR}{E}(1-e^{-\tau_a})\,e^{-\tau}\,e^{-\tau_w}}{1-e^{-2\tau}} \tag{36}$$

When the attenuation of the waveguide components can be neglected as compared with one of the accelerator, eq.(36) becomes

$$M = \frac{\sqrt{\frac{I^2R^2}{E^2}(1-e^{-\tau_a})^2 + (1-e^{-2\tau_a})} - \frac{IR}{E}(1-e^{-\tau_a})\,e^{-\tau_a}}{1-e^{-2\tau}} \tag{37}$$

(2), for constant gradient structure

For the constant gradient accelerator structure, its shunt impedance R(z) and attenuation $\alpha_a(z)$ are not constant, so one can not use Eqs.(34) - (37). One must calculate M by other ways.

The first way, according to following procedure:

a), suppose source power is P and M=1,

b), for the first cavity input power is $P_1=M^2P$,

c), calculate output power using the power dissipation equation

$$\frac{dP_i}{dz} = -2\alpha_i P_{i-1} - IE_i \tag{38}$$

where P_i, E_i and α_i are power, electric field and attenuation in the No.i cavity, respectively.

d), one by one calculated until get output power of last cavity P_{end},

e), calculate transmission coefficient $T=\sqrt{(P_{end}/P_1)}$,

f), substitution of T value into Eq.(14) gets M,

g), repeat b) to f) until the difference of M by two times calculate less than a given value.

This method is for numeric calculation. For analysis one can use following way.

The second way, If we introduce the beam loading factor into eq.(32), the transmission coefficient T will include three parts, eq.(32) becomes

$$T = e^{-\tau_w} e^{-\tau_a} e^{-\tau_b} \qquad (39)$$

where $\tau_w = \tau_{ps} + \tau_{st} + \tau_{ow}$

τ_w is attenuation of waveguide parts in TWRR,

$$\tau_a = \int_0^{L_a} \alpha_a(z)\, dz$$

τ_a is one of accelerator structure and

$$\tau_b = \frac{I}{E L_a} \int_0^{L_a} \alpha_a(z)\, dz \int_0^{L_a} R(z)\, dz$$

τ_b is one of beam loading.

Table 3 lists multiplication factor M of our three kinds of accelerator sections under optimal coupling condition with 100mA beam loading by different calculations.

Table.3 Multiplication factor M calculated
(with beam loading)

Method	Buncher		Accelerator(1–3)		Accelerator(4–7)	
	0 mA	100 mA	0 mA	100 mA	0 mA	100 mA
First way	3.092	2.254	2.867	1.981	2.585	1.795
Second way	3.092	2.040	2.867	1.977	2.585	1.773

The table 3 shows that using second way to calculate the normal accelerator sections, the error is not so large, but for the buncher section the error is large because of beam bunch phase changed.

2-2-3, Q value of the TWRR with accelerator

In TWRR there is an accelerator section that is not a linear microwave component. Its resonant curve will be steepened. The dependencies of the phase on the frequency in the waveguide and in the accelerator are shown following, respectively,

$$d\varphi_w = \varphi_w \frac{\lambda_g^2}{\lambda_0^2} \frac{df}{f} \tag{40}$$

$$d\varphi_a = \varphi_a \frac{C}{V_g} \frac{df}{f} \tag{41}$$

For the TWRR with an accelerator section QL of TWRR is given by:

$$Q_L = \frac{f}{2\Delta f} = \frac{\varphi_w \frac{\lambda_g^2}{\lambda_0^2} + \varphi_a \frac{C}{V_{ga}}}{2 \arccos\left(\frac{4T\sqrt{1-C^2} - T^2(1-C^2)-1}{2T\sqrt{1-C^2}} \right)} \tag{42}$$

where C on the numerator is the velocity of the light and Vg is the group velocity in the accelerator. The meanings of other symbols have already been mentioned above. Q vs. C coupling coefficient of TWRR with accelerator section is shown on Fig.13 (b).

Table 4 lists Q values of our TWRR with accelerator section and RF window, respectively.

Table.4. Q value

	T	Q_0	Q_L
TWRR with RF window	0.9972	19983	1995(C=0.294)
TWRR with accelerator without beam loading	0.9438	19246	10979(C=0.294)
TWRR with accelerator with beam loading	0.8360	6230	2962(C=0.550)

3. Transient (Field build-up) in TWRR

Steady state conditions are not attained instantaneously in TWRR. Initially, the signal E_0 entering the directional coupler is divided, a faction, E_0C, going to the accelerator section and a fraction, $E_0\sqrt{(1-C^2)}$, going to the external dummy load. The residual part at the end of the accelerator section E_0CT is combined in the coupler with the source signal. With proper phase relation, the result will be an increase in the amount of signal entering the accelerator section and a decrease in the amount entering the external load. As the recirculation of the signal proceeds, the signal to the accelerator will continue to increase step by step and the signal to the load will continue to decrease until steady state conditions are reached. Fig.16 shows the electric field build-up process. Table 5 shows the magnitudes of each port during the recirculations for given T=0.9438, C=0.2939 and $\sqrt{(1-C^2)}$ =0.9558.

Table 5. Field build-up process

(power turn on)

Times	Port 1	Port 2	Port 4	Port 3
0	0	0	0	0
	$E_1 = E_0$	$E_2 = E_0\sqrt{1-C^2} - CE_3$	$E_4 = E_3\sqrt{1-C^2} + CE_0$	$E_3 = TE_4$
1	E_0	$0.9558E_0$	$0.2939E_0$	$0.2774E_0$
2	E_0	$0.8743E_0$	$0.5590E_0$	$0.5276E_0$
3	E_0	$0.8007E_0$	$0.7981E_0$	$0.7532E_0$
4	E_0	$0.7344E_0$	$1.0138E_0$	$1.0395E_0$
⋮	⋮	⋮	⋮	⋮
∞	E_0	$0.1229E_0$	$3.0030E_0$	$2.8314E_0$

(power turn off)

Times	Port 1	Port 2	Port 4	Port 3
0	E_0	$0.1229E_0$	$3.0030E_0$	$2.8314E_0$
	$E_1 = 0$	$E_2 = 0 - CE_3$	$E_4 = 0 + E_3\sqrt{1-C^2}$	$E_3 = TE_4$
1	0	$-0.8320E_0$	$2.706E_0$	$2.554E_0$
2	0	$-0.7506E_0$	$2.441E_0$	$2.304E_0$
3	0	$-0.6771E_0$	$2.202E_0$	$2.078E_0$
4	0	$-0.6108E_0$	$1.986E_0$	$1.875E_0$
⋮	⋮	⋮	⋮	⋮
∞	0	0	0	0

The field build-up in TWRR is a stepwise process with intervals between steps equal to the ring transit time.

$$t_f = \frac{L_a}{V_{ga}} + \frac{L_w}{V_{gw}} \tag{43}$$

The time constant is given by

$$T_f = \frac{Q_0}{\omega} \tag{44}$$

The time required to build-up to a 99.9% of the steady state value is $T = 7\,T_f$. The number of transits required to build up to a 99.9% of the steady state value is given by

$$N_f = \frac{7\,T_f}{t_f} \tag{45}$$

For our case these values are shown on the table 6

Table 6. Parameters of transient

	C	M	Q_0	t_f (μs)	T_f (μs)	T (μs)	N_f
TWRR with RF window	0.294	6.33	19983	0.021	5.00	35.0	1669
TWRR with Acc. (without. beam loading)	0.294	3.01	19983	0.274	2.75	19.3	70
	0.550	2.52	4254	0.274	1.08	7.58	28
TWRR with Acc. (with beam loading)	0.294	1.43	4841	0.274	1.23	8.63	32
	0.550	1.80	5800	0.274	0.73	5.07	18

The transient in TWRR is not so important for CW or long pulse operation because it transient time can be neglected as

compared with the pulse lasted time. But it is important for short pulse.

Until now we have not measured yet. In the near future it will be measured, and the data will be checked.

4. Result and discussion

4-1, low power test

4-1-1, TWRR with accelerator section test

Figure 17 shows TWRR with accelerator section at the low power test system. TWRR has a main directional coupler that has four ports: port 1 connects with a RF window and TC1 (transformer connector) which connects to the signal source, port 2 connects with another RF window, a Bathe-hole coupler C4 and a dummy load, port 4 and port 3 connect to the resonant ring, which includes another Bathe-hole coupler C3, a stub tuner, an accelerator section, a phase shifter and a waveguide had a vacuum connector.

The main directional coupler has a 10dB coupling coefficient and 39dB directivity. The Bathe-hole couplers have a 60dB coupling coefficient and larger than 26dB directivity.

A network analyzer is used conveniently for measurement. The signal from the network analyzer passes through TC1 into the port 1 of the directional coupler. The signals picked from forward and backward of the Bathe-hole coupler C3 which is located at the port 4 are measured as forward and backward electric field in TWRR, respectively. And the signal picked from forward of the Bathe-hole coupler C4 which is located at the port 2 is measured as the electric field to the dummy load. These electric fields measured include both of the amplitude and phase.

According to the network analyzer functions, using "S11" function one can get VSWR in the port 1. Using "S21" one can get the multiplication factor M and nullification factor N by connecting to C3 and C4, respectively. And using "PHASE" one can get the phases of M and N, respectively.

Before tuning and matching TWRR, M, N, VSWR and reflection in the ring are shown on the Figs.18, 19, 20 and 21, respectively. One can see that there is large reflection in the ring, so multiplication factor M is low and has two peaks, N and VSWR are large. M and N have two peaks.

After adjusting the phase shifter to make TWRR resonance and adjusting the stub tuner to make TWRR matching, one can get following data M, N, VSWR and reflection power in the resonant ring which are shown on the Figs.22, 23, 24 and 25, respectively. One can see that there is small reflection in the ring, therefore, M becomes large and only one peak at resonance, N and VSWR become small.

From Fig.22 one can find mark 1 loss D=50.807dB, using following formula to get M:

$$M = 10^{(\frac{60-D}{20})} = 2.88 \qquad (46)$$

and Q value Q =10537.

4-1-2, TWRR with RF window test

Figure 26 shows TWRR with RF window at low power test system. There is a stub tuner for matching the ring. There is no phase shifter, but some spacers to change the length of the ring to make the ring near the resonant point, then adjusting the frequency to tune the ring at resonance.

M and N are shown on the Fig.27 and Fig.28. Its M=6.33 and Q=1956.

4-2, High power test

4-2-1, TWRR with accelerator section

At first the TWRR included the stub tuner and phase shifter to do the high power test. Because the phase shifter had a large loss, in a plunger choke part became heating and made a lot of discharge, one could not input the power more than 50KW in the resonant ring. Therefore, a straight waveguide is used instead of the phase shifter. As mentioned above, using some spacers and adjusting frequency the TWRR can be tuned at resonance.

Figure 29 shows TWRR with accelerator section under the high power test system, respectively. A CW klystron made in Toshiba is used for RF source. When the RF power passes through the magic T, it will be divided equal two parts: one half power transmits to TWRR, another half passes a stub tuner and reaches to the dummy load. This stub tuner is to cancel the reflection

from TWRR. There are four Bathe-hole couplers: C1 is located between the klystron and magic T, it can measure klystron output power by power-meter and reflection power which connects interlock system to protect the klystron against the reflection, C2 is located between the magic T and TWRR, it can measure TWRR input power by power-meter and reflection from TWRR which connects to interlock system too, C3 is inserted TWRR to measure forward and backward power in TWRR by power-meter to get multiplication factor and reflection in TWRR and C4 is located between the main coupler and the dummy load to measure the power reached the dummy load by power-meter to get nullification factor. To get phase of M and N one can measure phase differences between C2 and C3 and between C2 and C4 by phase-meter, respectively. Figs. 30 and 31 show M , θ and N ,φ vs. frequency f, respectively. Fig. 32 shows M vs. P_{in}. Fig.34 shows forward and backward power in TWRR vs. f for different reflection Γ, respectively.

From Figs.30 and 31 one can see that when the frequency changing from low to high the resonant curve becomes sharp, when the frequency changing from high to low the resonant curve becomes dull. They are caused by the accelerator thermal characteristic. Their average values are real values.

Fig.32 shows that when input power changes the multiplication factor M can keep constant by changing frequency f to make the ring at resonance.

Fig.33 shows that before one adjusts the plunger of the stub tuner, the reflection in the ring is larger and the multiplication factor is very low and has two peaks. After one adjusts it, the reflection becomes lower and lower,therefore, the multiplication factor M becomes higher and higher. This means that the stub tuner can match the ring successfully.

The thermal characteristics of the accelerator are shown on Fig.34.

$$dT/dP_{ring} = 2.4^\circ /100KW$$

$$df/dP_{ring} = -57.5\ KHz/100KW$$

and $$df/dT = -24KHz/1^\circ c \quad .$$

On the resonant curve of TWRR the right side is stable, but the left side is unstable. It is shown on Fig.35. Let's suppose that the operation frequency is higher then the resonant frequency of TWRR. It includes two cases: in one case, TWRR resonant frequency is fo, but the operation frequency is fo+Δf1

(at B point); in another case, the operation frequency is fo, but the resonant frequency of TWRR is fo-Δf1 (at B' point). The result is the same for both. we only analyse one case. When the temperature becomes lower, TWRR resonant frequency will be higher, this means that the resonant curve will move towards the right, so M becomes higher, the resonant power will be higher too, the temperature will return to its original value. Therefore, this right side is stable. Supposing that operation frequency is lower then the resonant one (at C or C' points), when the temperature becomes lower, it will be lower and lower, so this left side is unstable. In this side if the temperature or resonant power becomes higher, the operation point will return to the resonant point (A point).

TWRR operates at the resonant point (at A point), the resonant curve $dP_r/df=0$, therefore, this is stable point, if the temperature, phase and frequency are controlled within a reasonable accuracy.

4-2-2, TWRR with test RF window

Figure 36 shows the Rf window high power test system, using long pill box in which the window is made of BeO ceramic, that has a low RF loss and high thermal conductivity, one put input CW power is 44KW and get CW power 1.7MW in the resonant ring. The multiplication factor is 6.22 that is good agreement with low power test. Fig. 37 shows thermal characteristics of three kind window. The long pill box with BeO ceramic window is the best one. This RF window is designed for CW 1.2MW klystron. The result is very good.

5. Summary

For TWRR with accelerator section, the data from calculation, low power measurement and high power measurement are listed at the Table 7. The multiplication factor M dependence on the reflection Γ from calculation and high power test measurement are listed at the Table 8. Table 9 lists the accuracy requirement of the TWRR with accelerator section.

Table 7. Results of TWRR

	Theoretic Calculation Value	Low power Measurement Value*	High power Measurement Value
M	3.02	2.90	3.03
$d\theta / d\varphi$	9.22	8.20	9.00
N	0.123	0.16	0.12
$d\psi / d\varphi$	68.71	50.4	70.2
Q	10797	10601	11478

* At low power measurement case TWRR including the phase shift has high attenuation, so multiplication factor M a little bit low.

Table 8. M dependence on reflection

Γ	Calculation		Measurement (high power)	
	M	Γ_{ring}	M	Γ_{ring}
0	3.00	0.0	3.02	0.09
0.029	2.793	0.295	2.87	0.24
0.053	2.405	0.534	2.47	0.46
0.074	2.030	0.737	1.65	0.73

Table 9. Accuracy requirement

Frequency f	1249.135 ± 0.001 MHz
Resonant ring phase φ	360° n ± 0.5°
Temperature T	40 ± 0.1° C
Klystron voltage V_k	90 ± 0.1 KV

From the Tables 7 and 8, one can see that the parameters of TWRR with accelerator section are very good agreement between the calculation and measurement data. This means that most of these formulae without beam loading have been checked. Those formulae with beam loading will be checked in the future beam test. According to the high power test this TWRR with accelerator section can operate stably at resonance and under optimal efficiency condition.

6, Acknowledgements

Author wishes to thank Prof. I.Sato, who gave author very good directions and helpful discussions and to thank Dr.M.Ono and all of our accelerator group members who did a lot of jobs for the experiments and gave helpful discussions. Author is very much indebted to our leaders Dr.Sasao, Dr.Himeno and Dr.Sakuma who gave author a good research condition and good guidances.

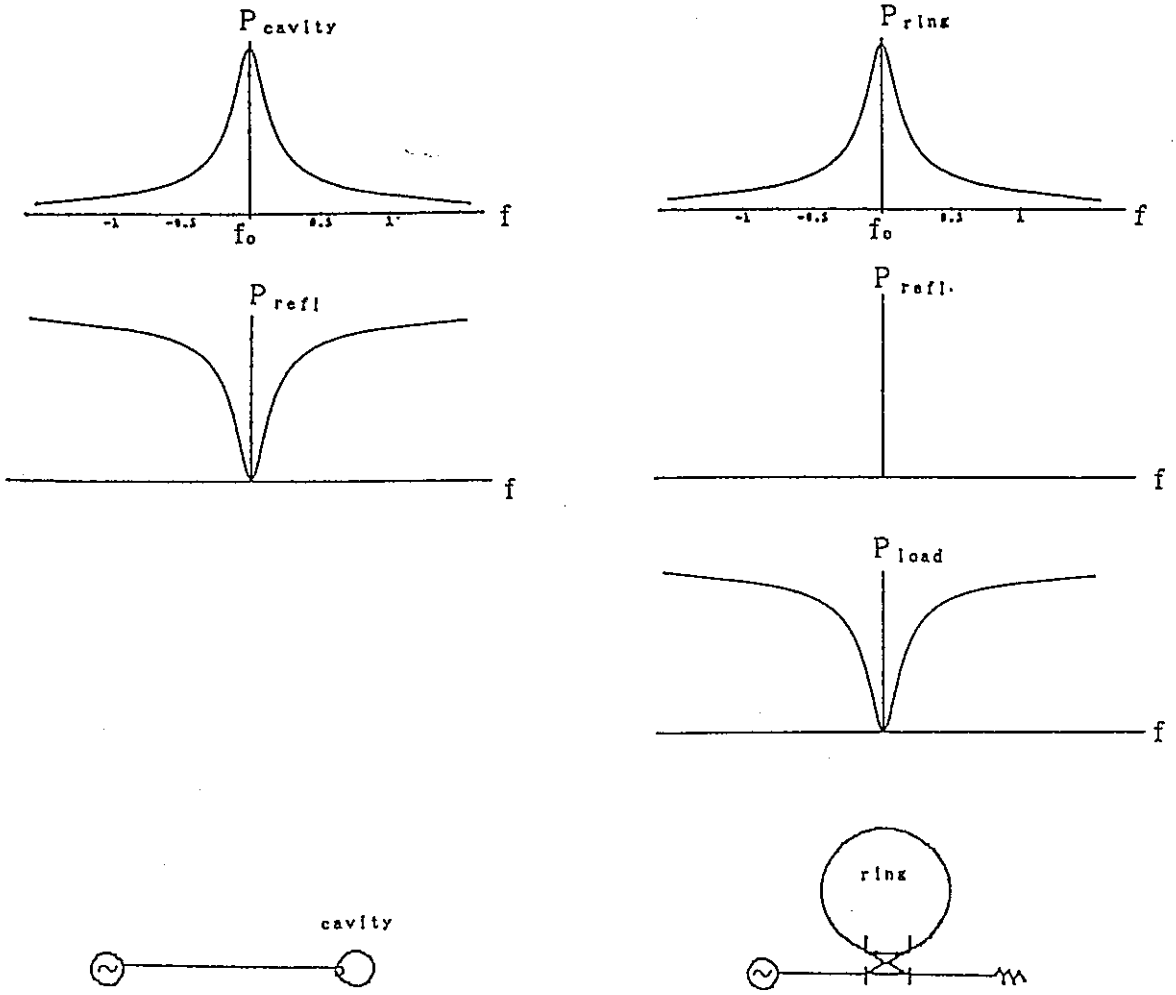

(a), standing wave resonant cavity (SWRC)

(b), traveling wave resonant ring (TWRR)

Fig.1, Frequency characteristics of SWRC and TWRR

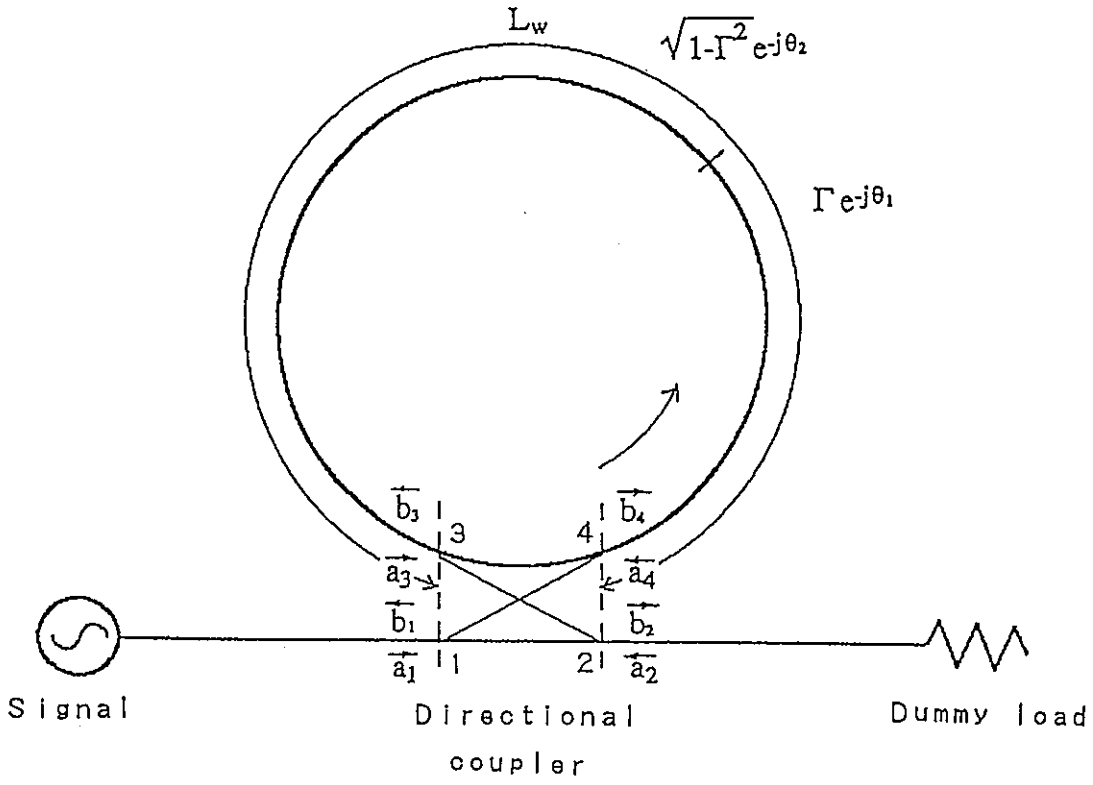

Fig.2, A simple TWRR

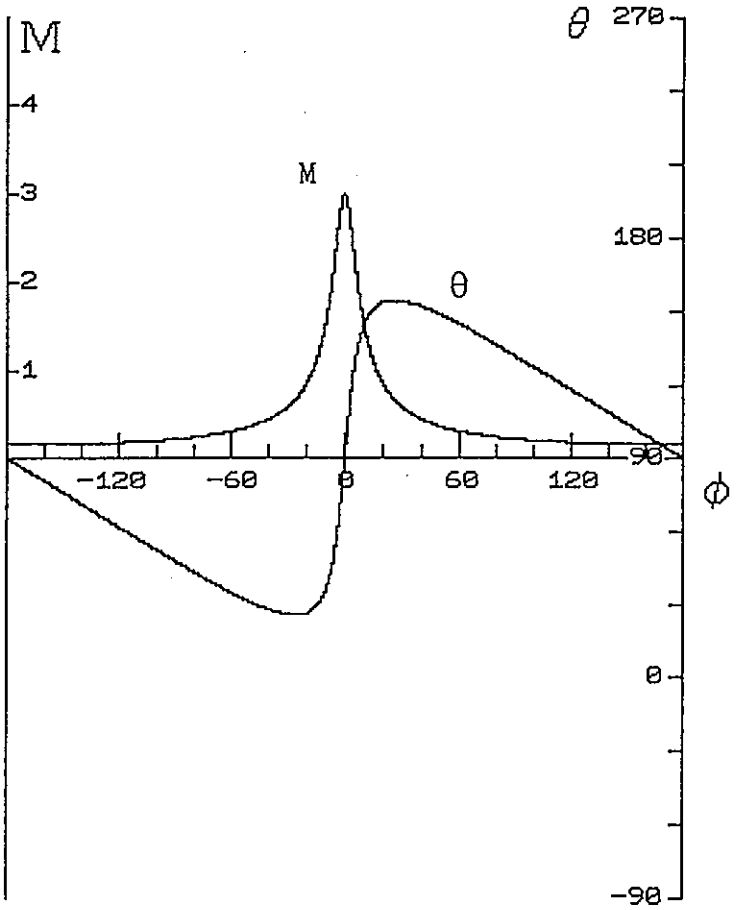

Fig.3, M vs. φ and θ vs. φ for C=0.2939 and T=0.9438

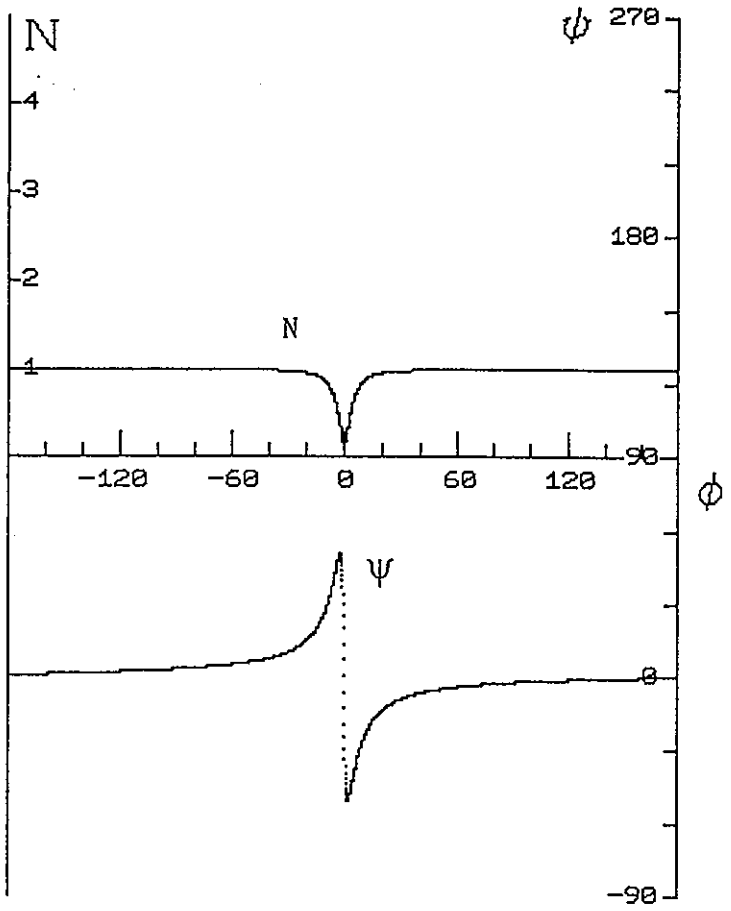

Fig.4, N vs. φ and ψ vs. φ for C=0.2939 and T=0.9438

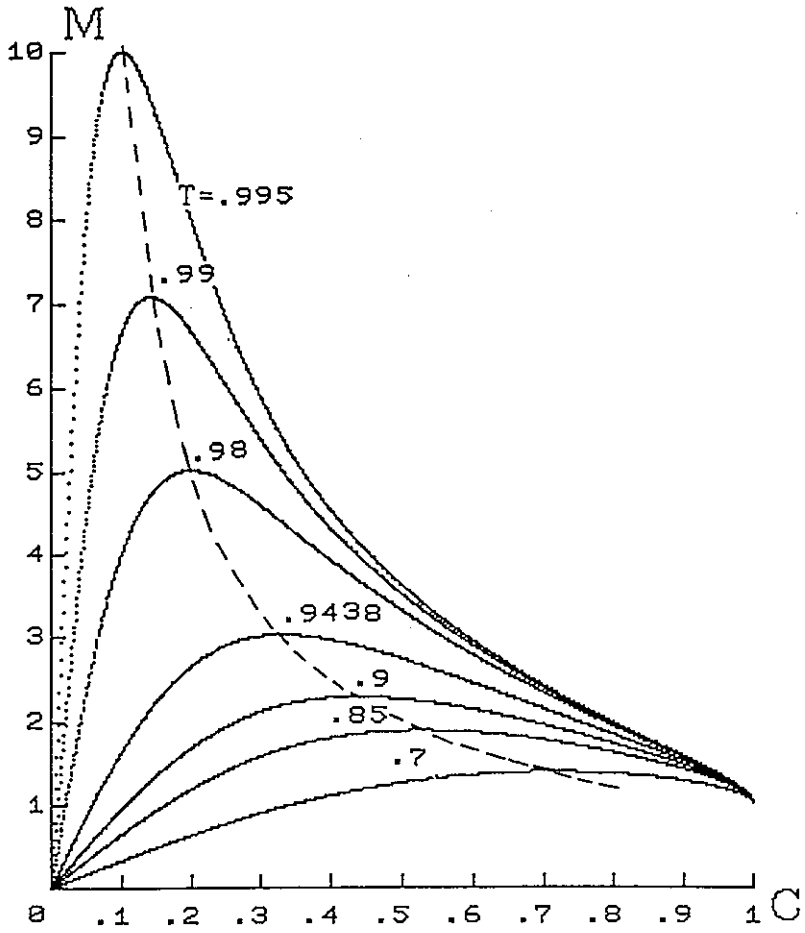

Fig.5, M vs. C at the resonance for different T

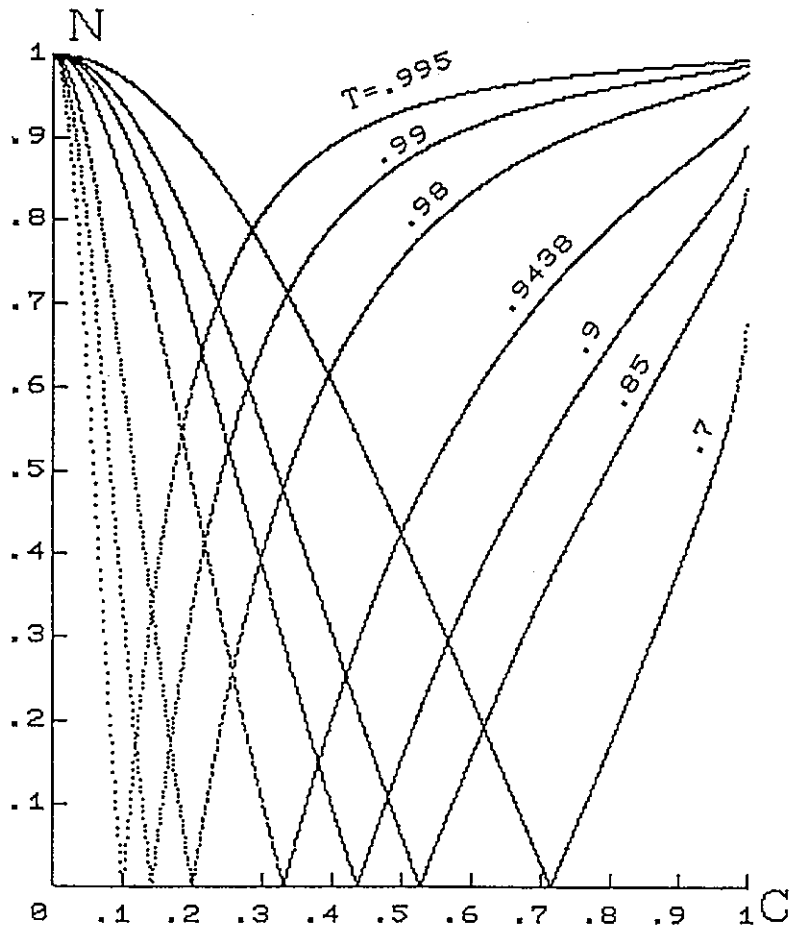

Fig.6, N vs. C at the resonance for different T

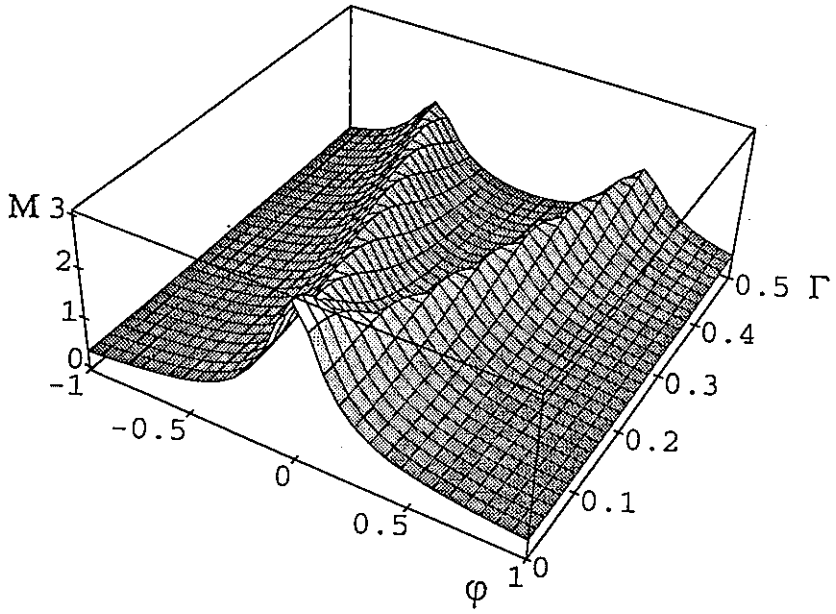

Fig.7, 3-dimensions graph of M vs.φ and Γ

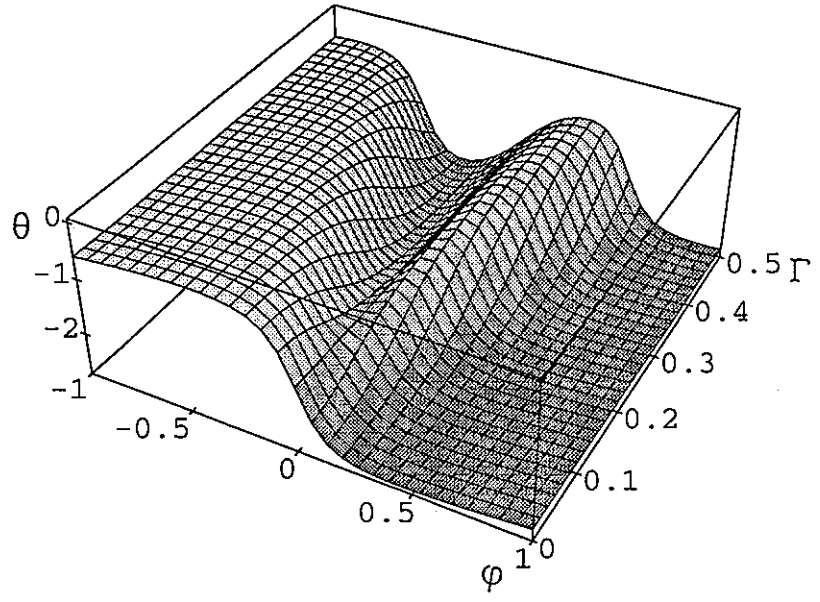

Fig.8, 3-dimensions graph of θ vs.φ and Γ

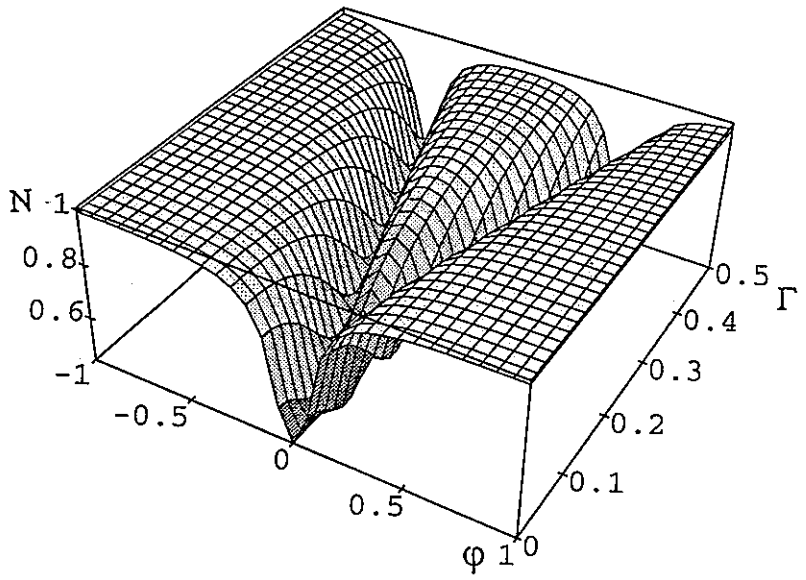

Fig.9, 3-dimensions graph of N vs. φ and Γ

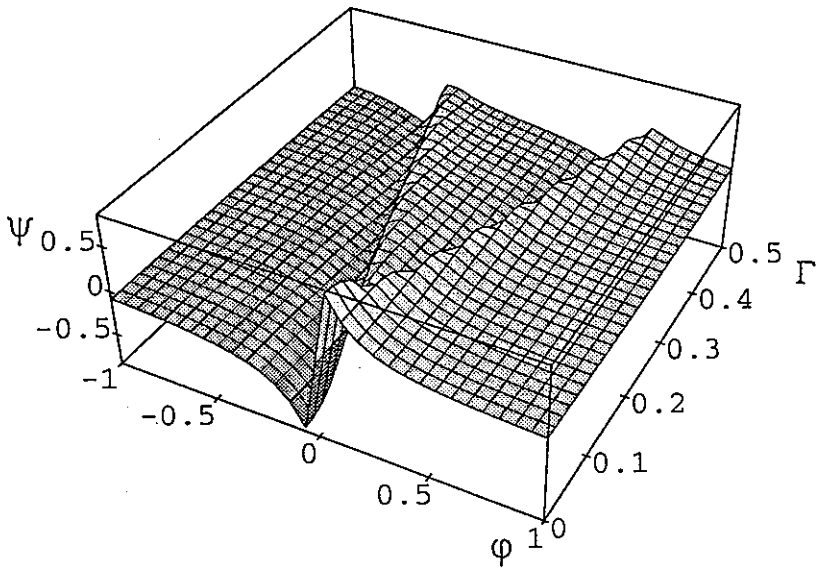

Fig.10, 3-dimensions graph of ψ vs. φ and Γ

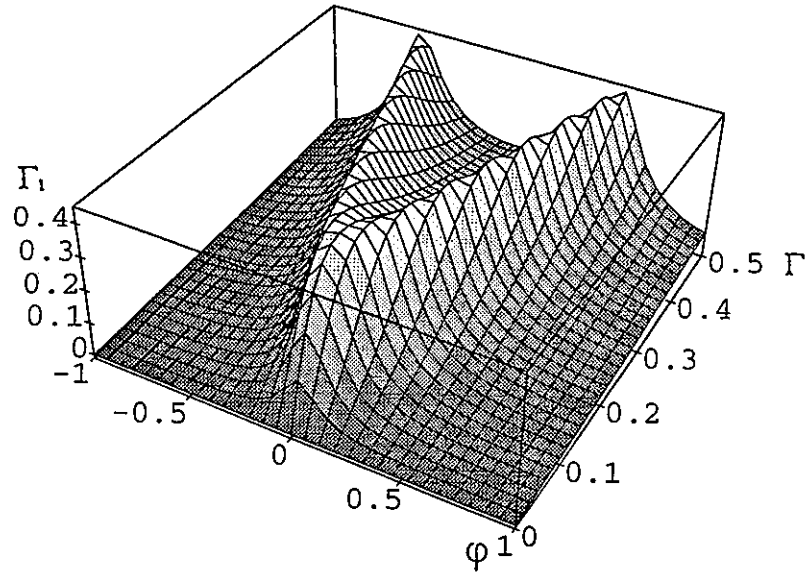

Fig.11, 3-dimensions graph of Γ_1 vs. φ and Γ

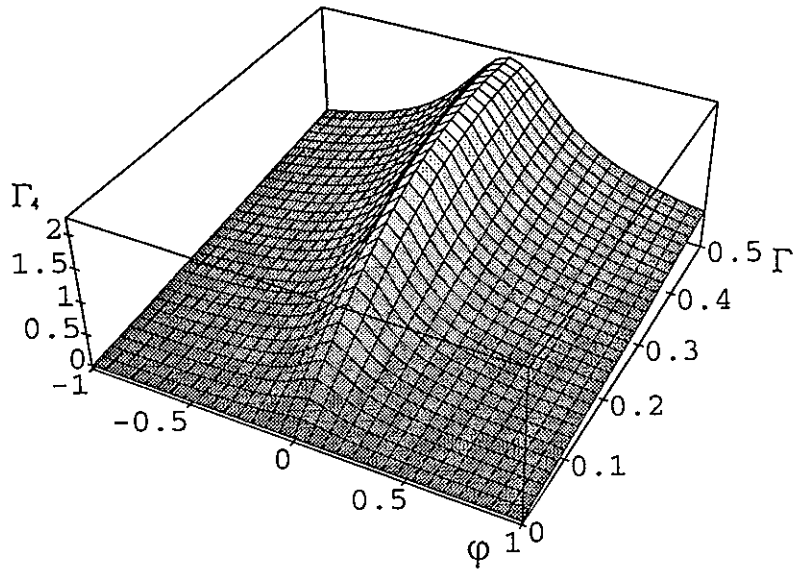

Fig.12, 3-dimensions graph of Γ_4 vs. φ and Γ

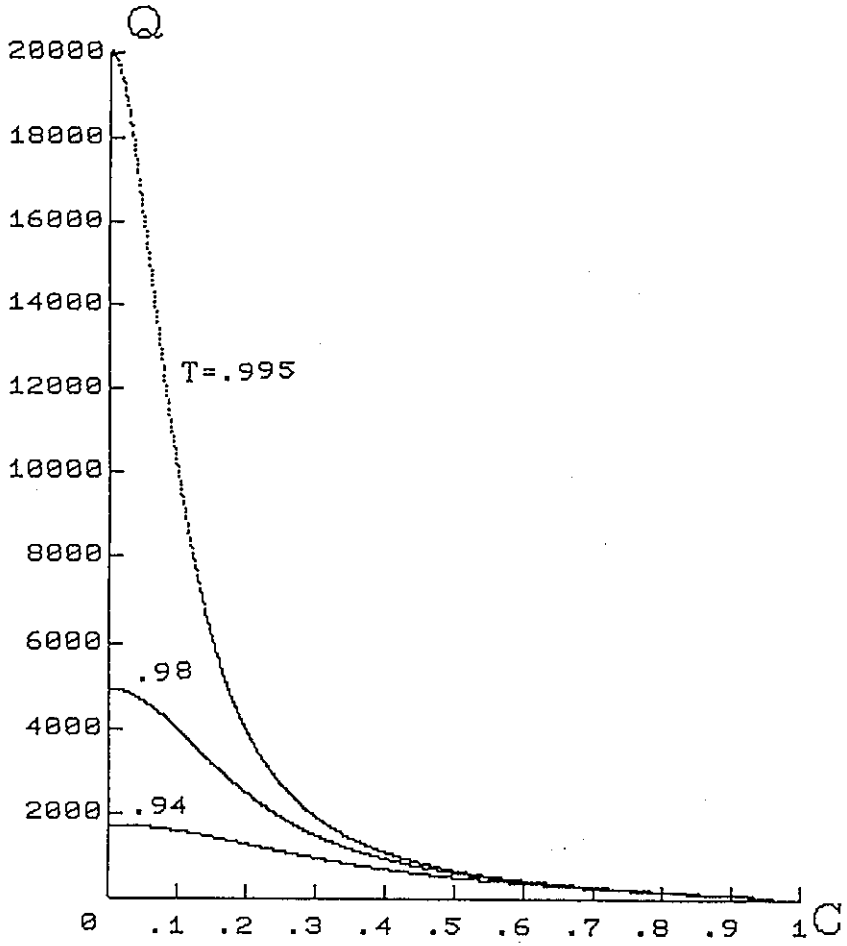

(a), for a simple TWRR

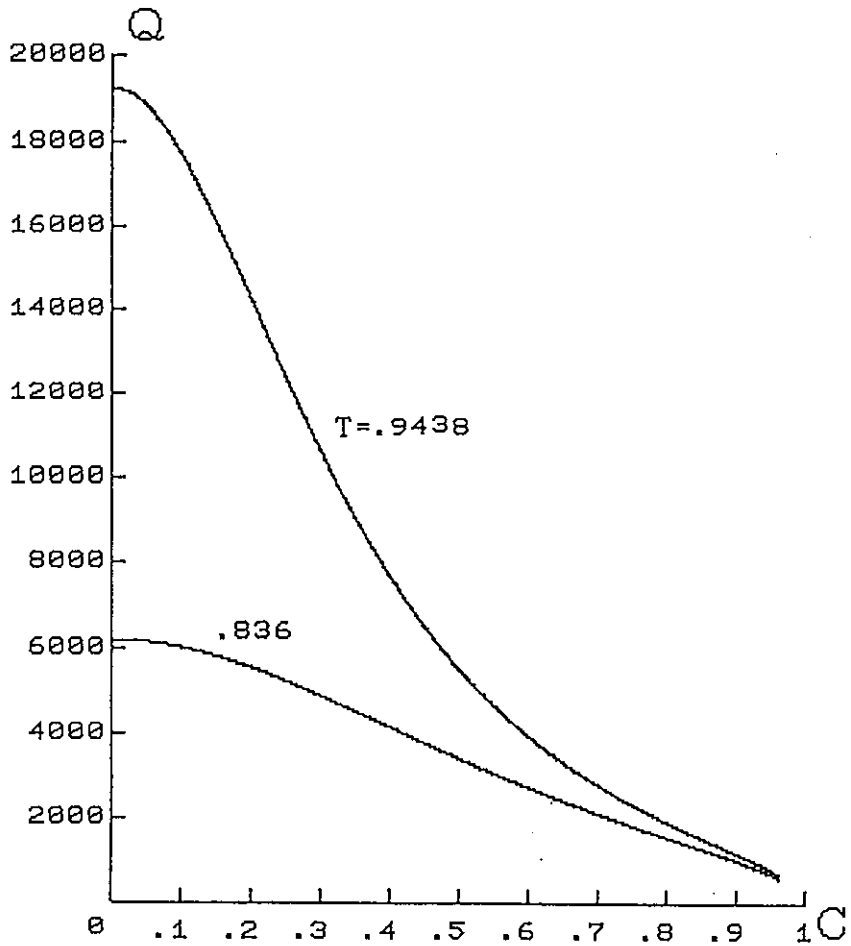

(b), for TWRR with the accelerator

Fig.13, Q vs. C for different T

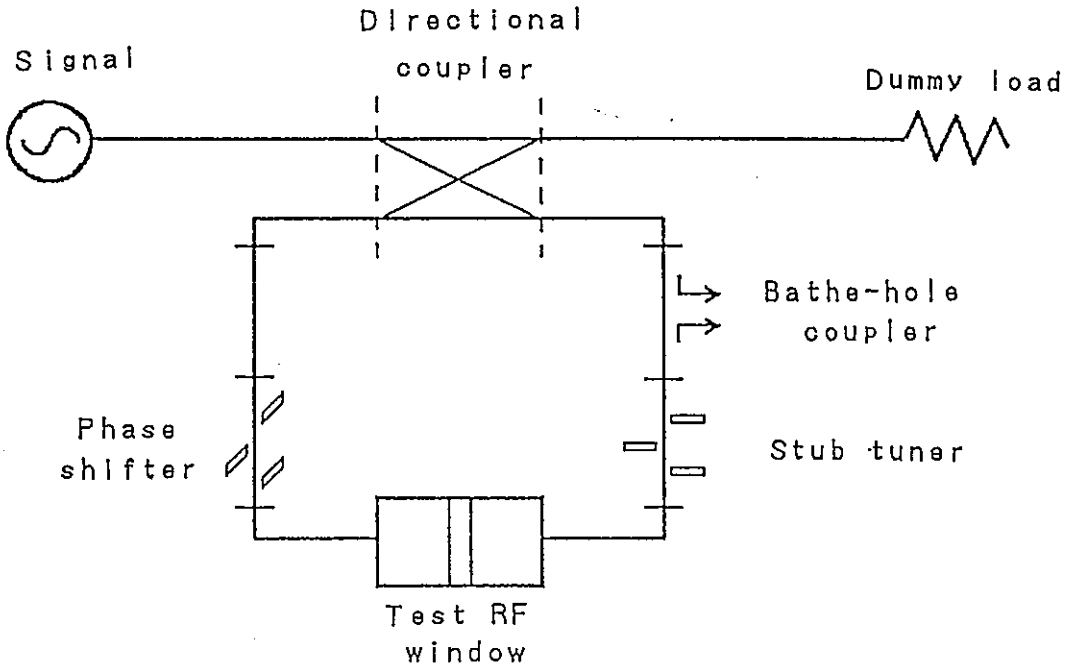

Fig.14, A TWRR with a test RF window

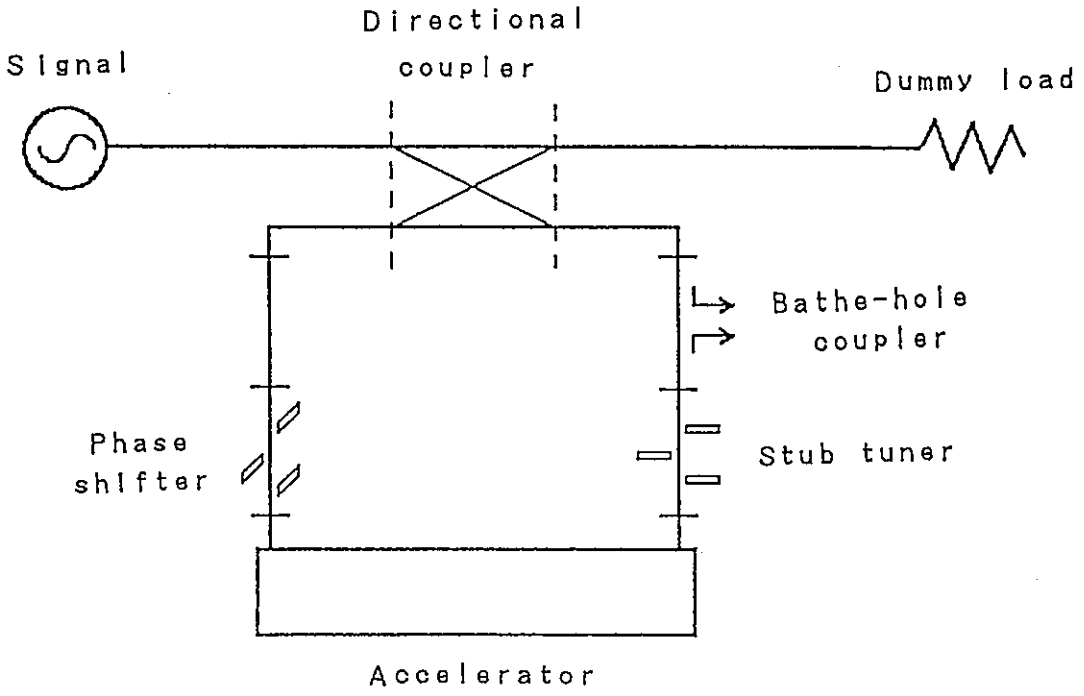

Fig.15, A TWRR with an accelerator section

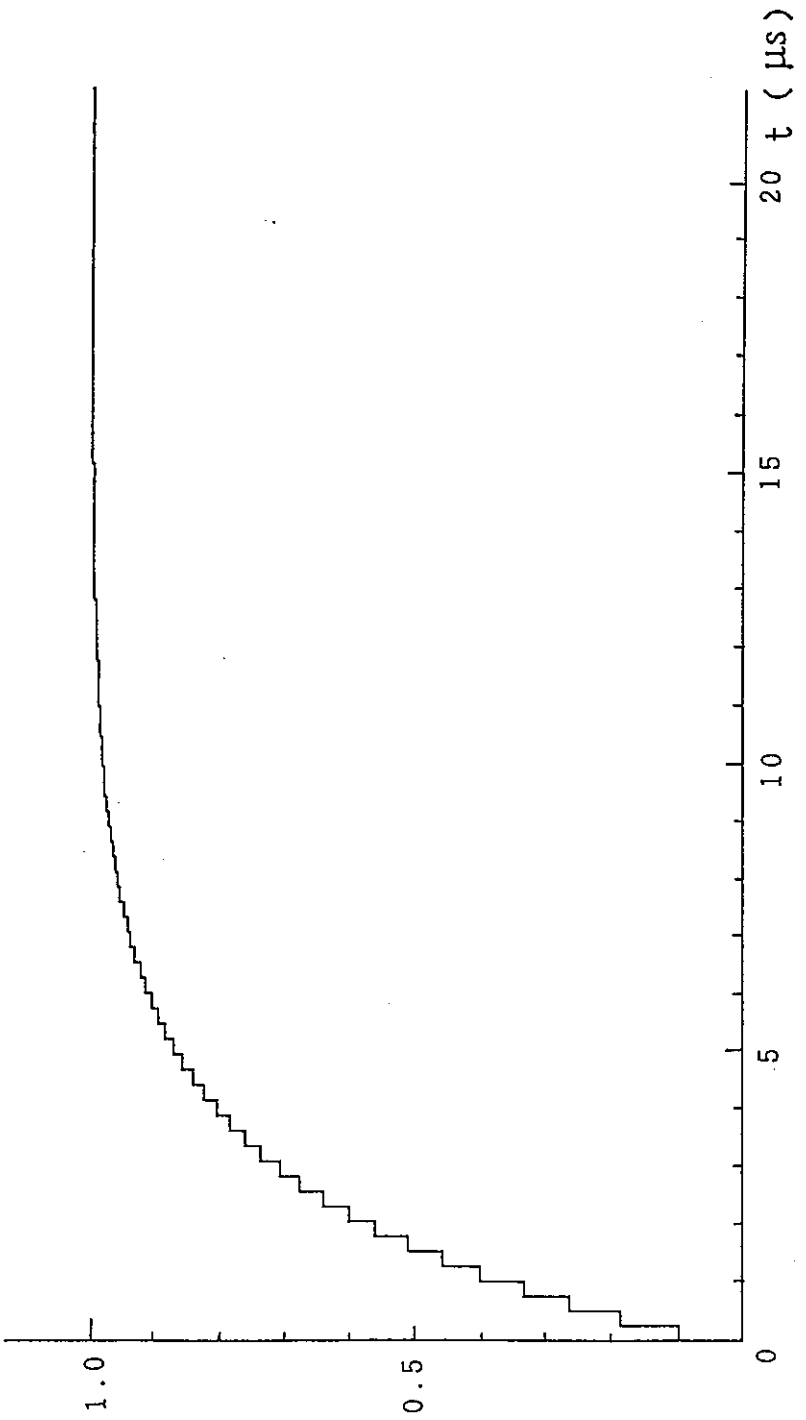

Fig.16, Field build-up in TWRR for C=0.2939 and T=0.9438

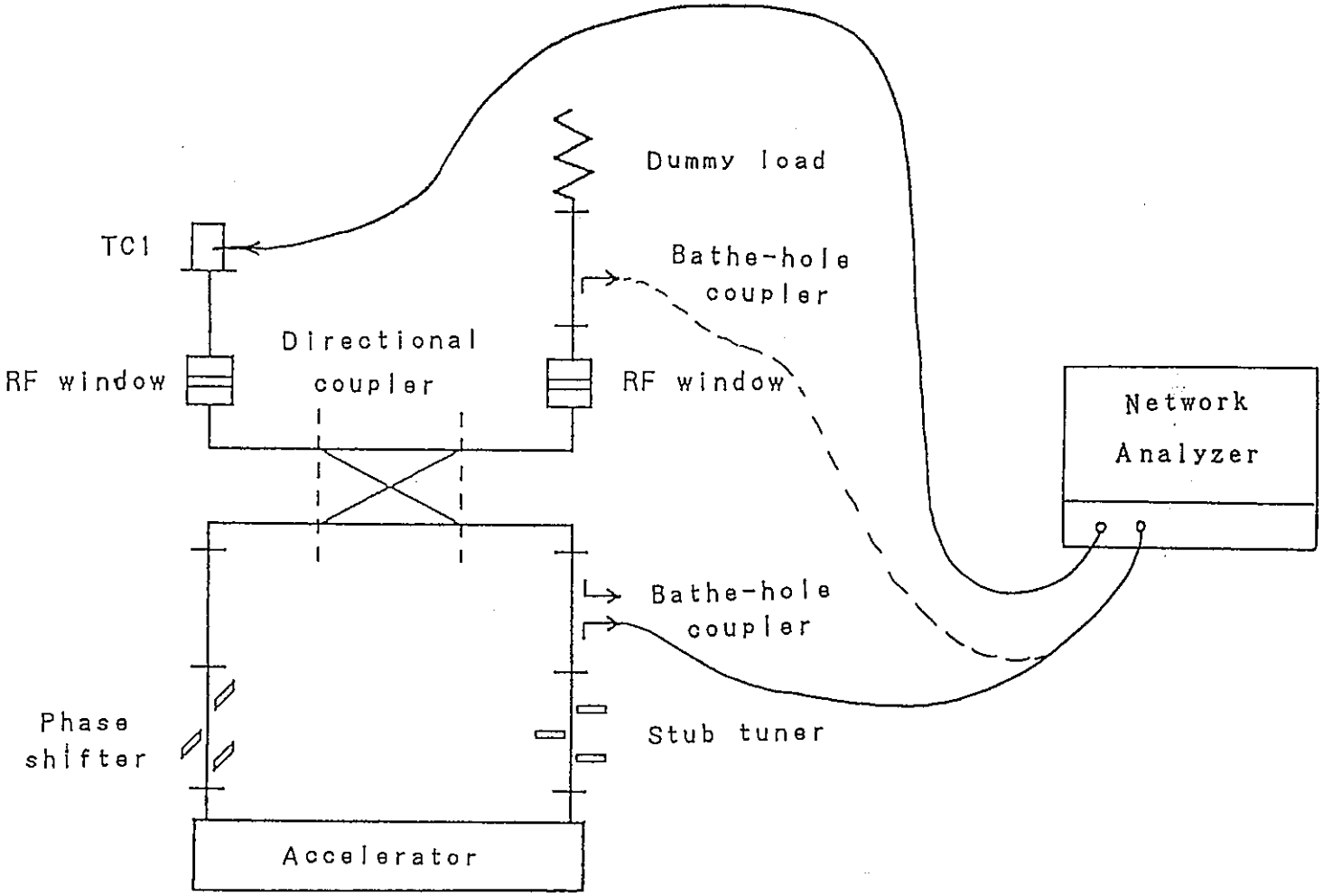

Fig.17. The low power test system for TWRR with the accelerator section

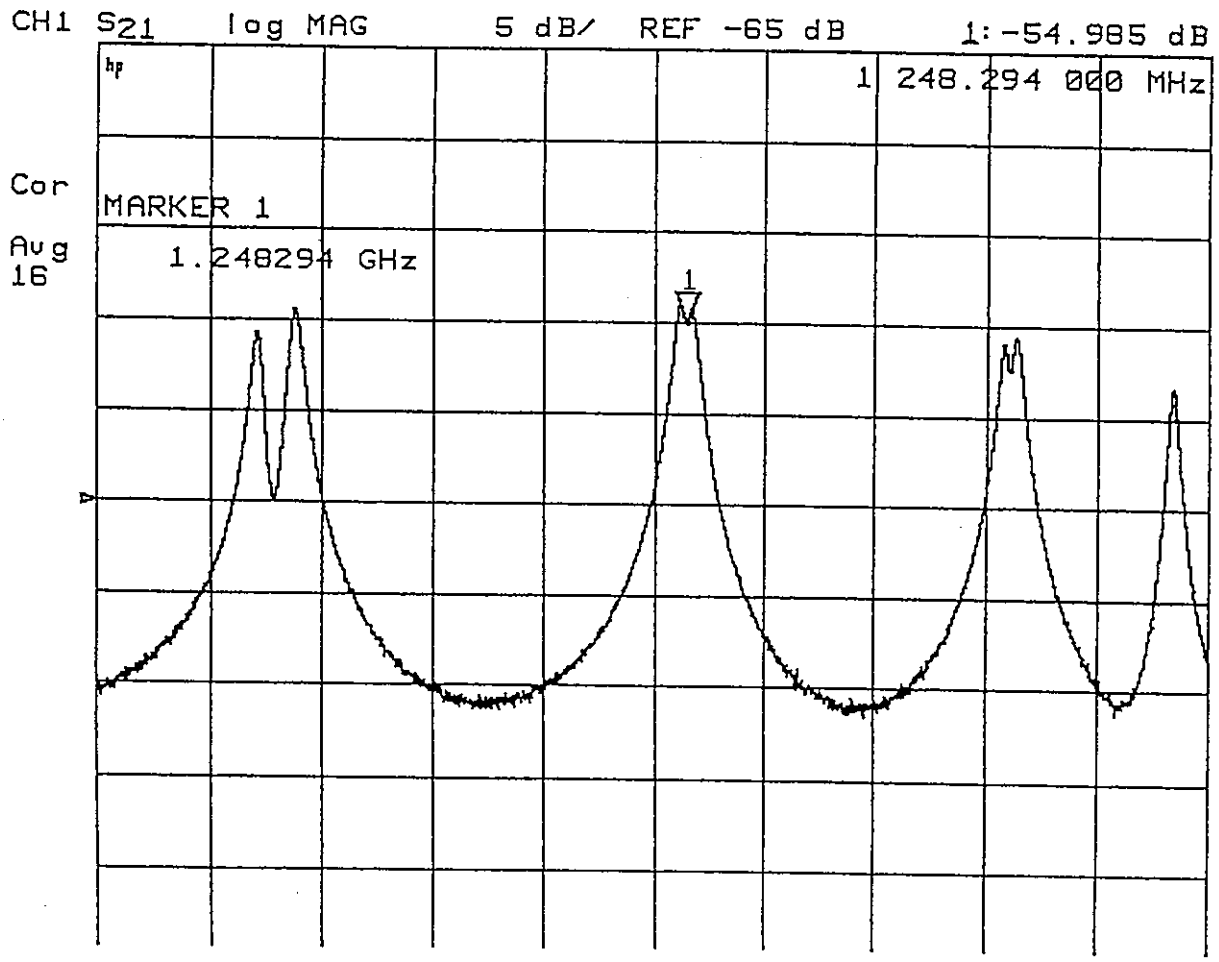

Fig.18, P3f vs. f measured before tuning and matching for TWRR with the accelerator section

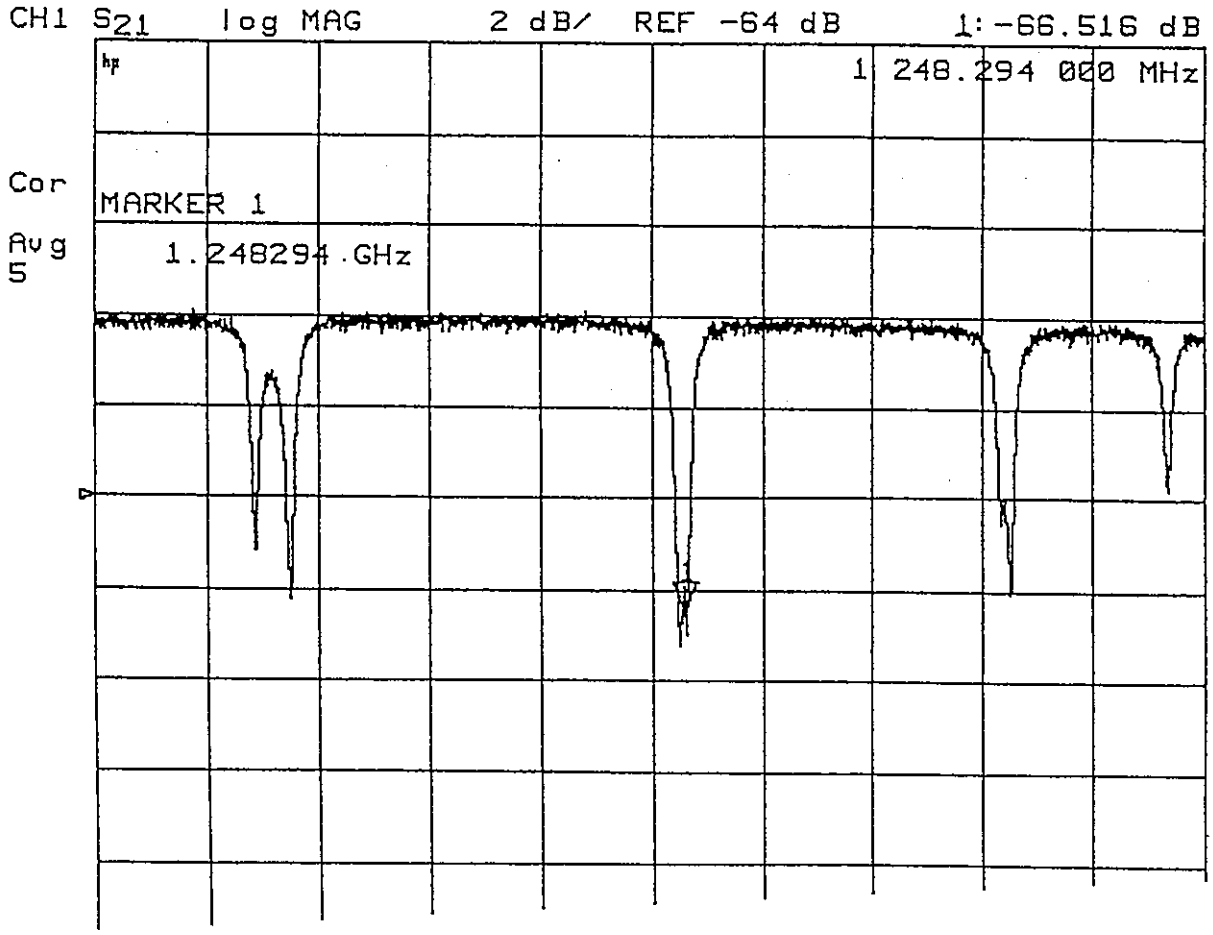

Fig.19, P4f vs. f measured before tuning and matching for TWRR with the accelerator section

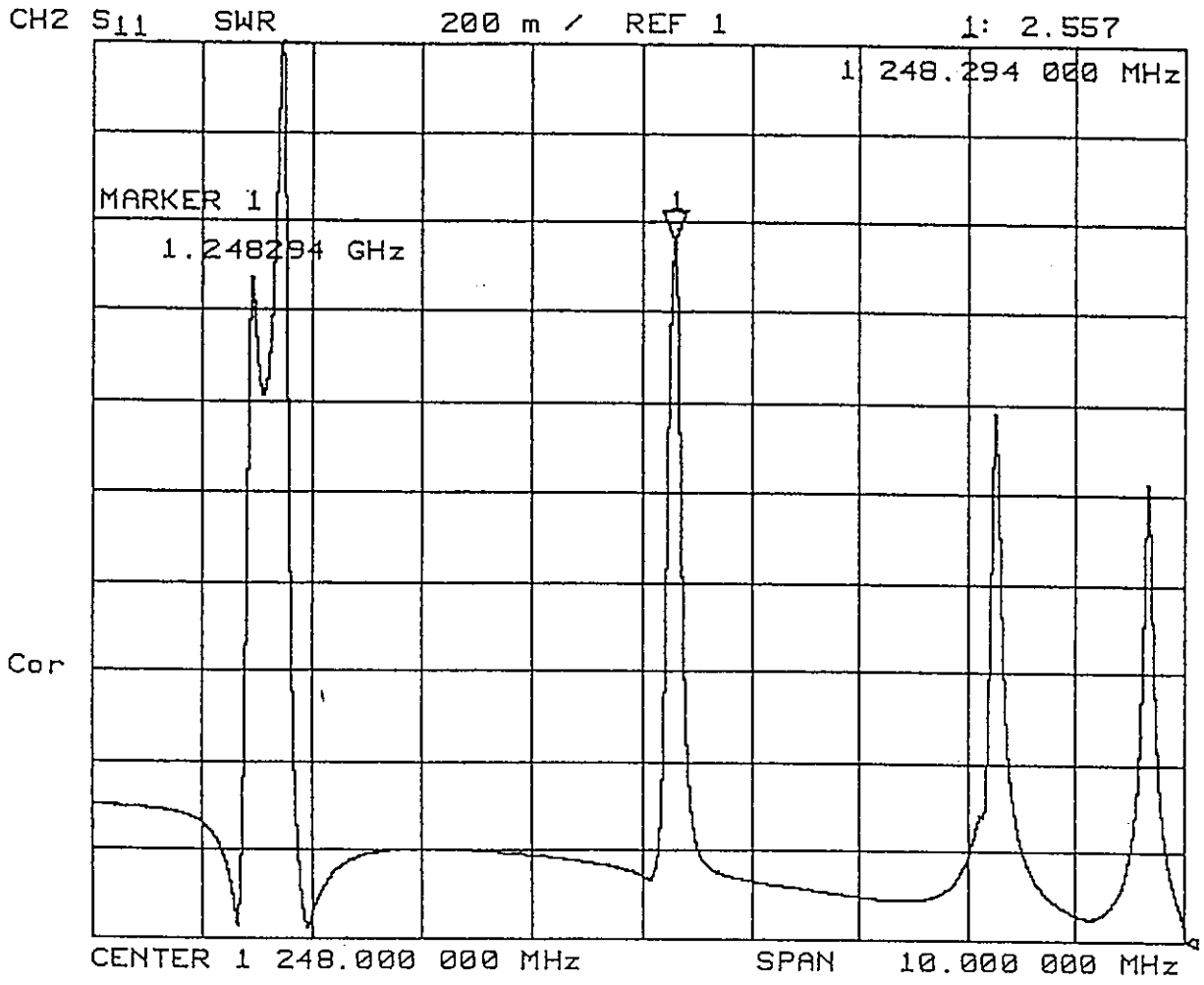

Fig.20, VSWR vs. f measured before tuning and matching for TWRR with the accelerator section

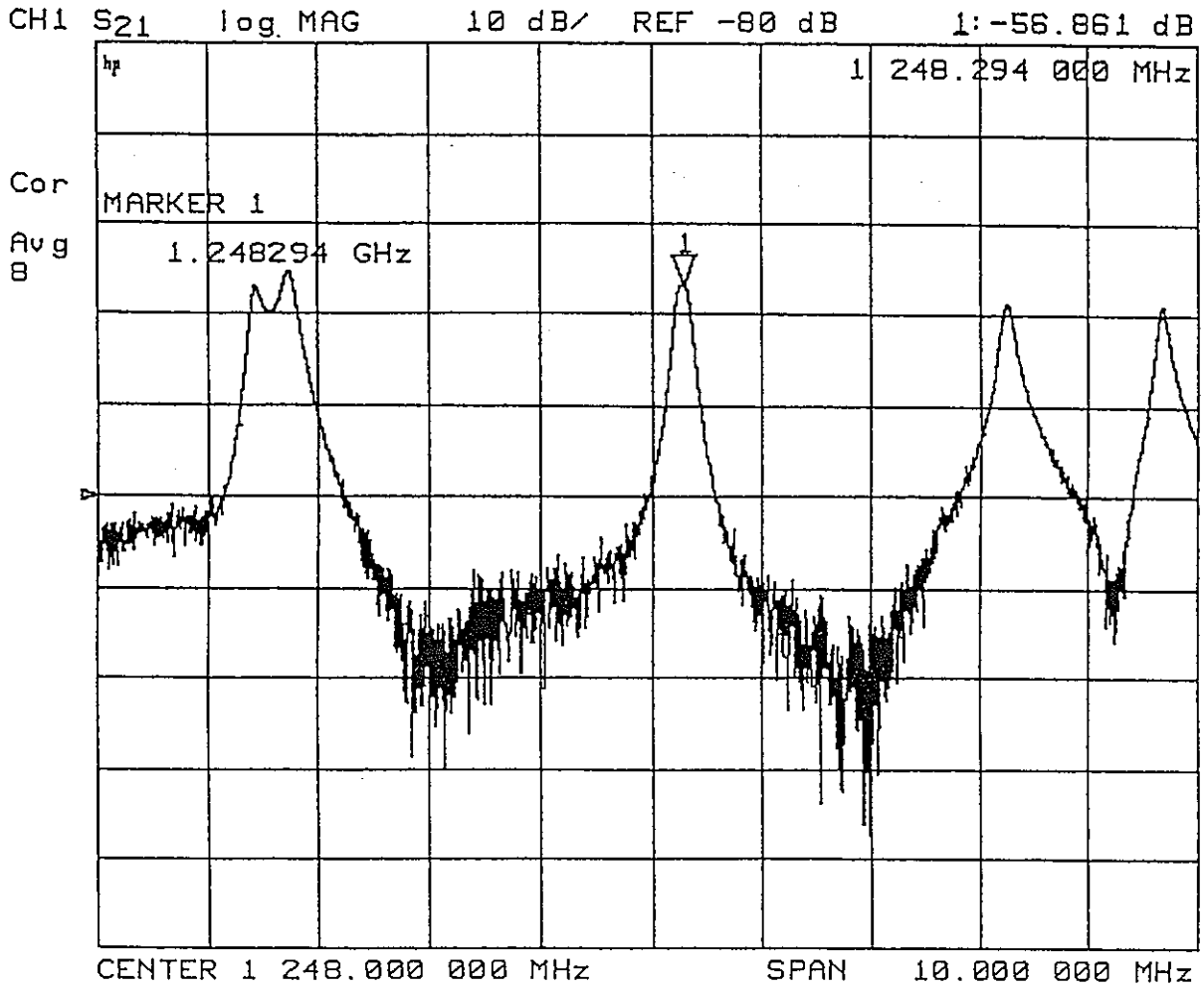

Fig.21, P3b vs. f measured before tuning and matching for TWRR with the accelerator section

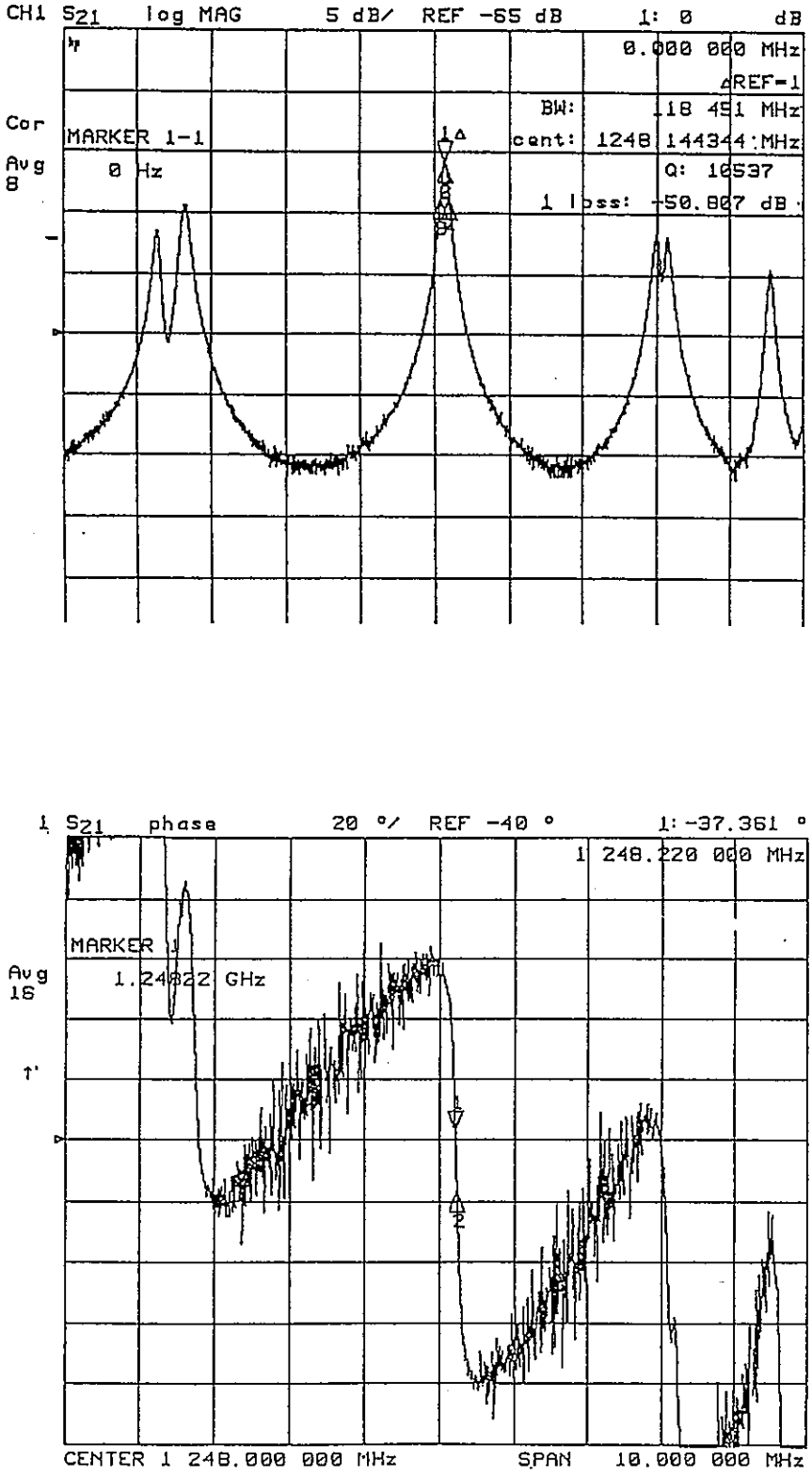

Fig.22, P3f vs. f and θ vs. f measured after tuning and matching for TWRR with the accelerator section

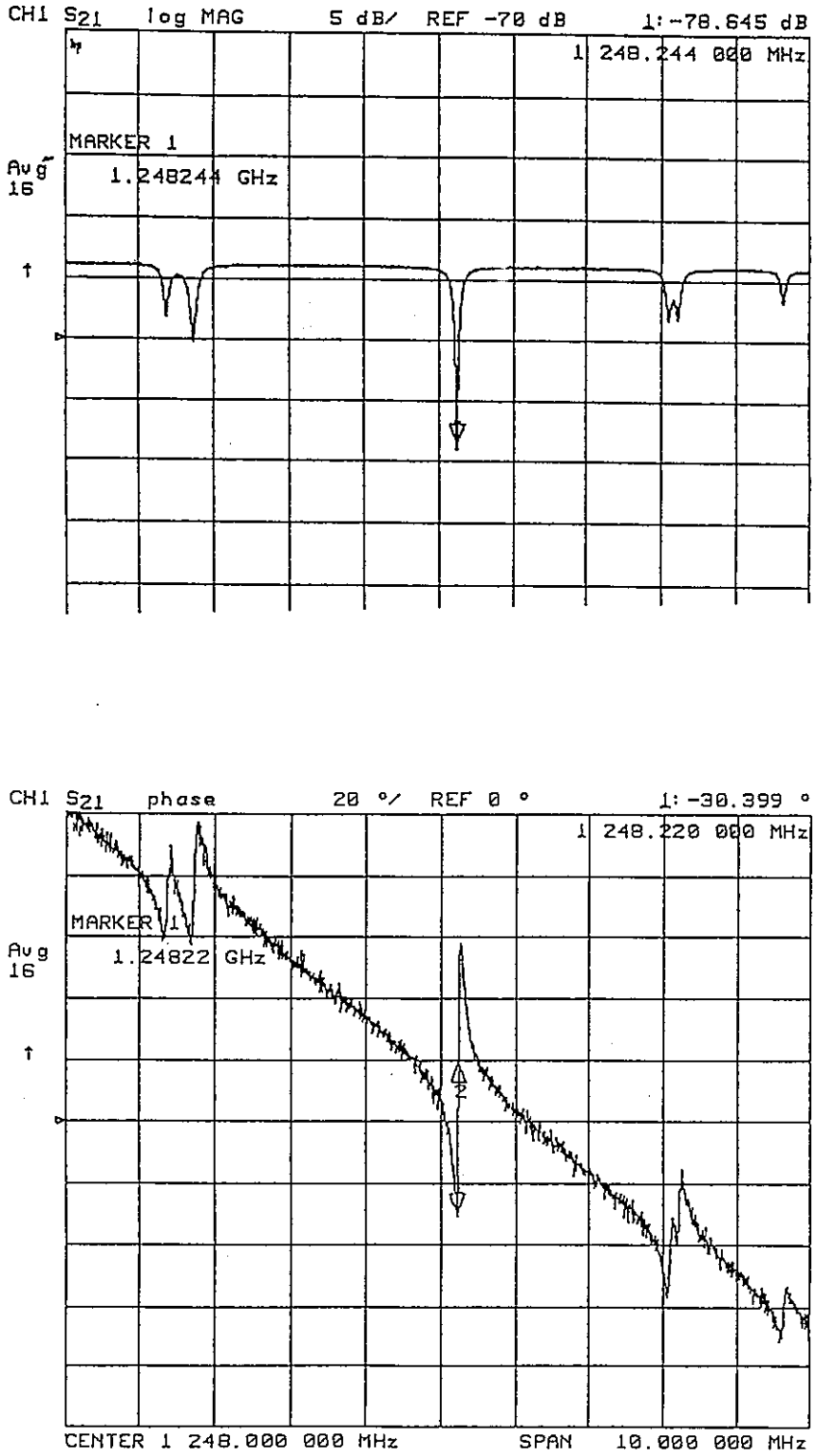

Fig.23, P4f vs. f and Ψ vs. f measured after tuning and matching for TWRR with the accelerator section

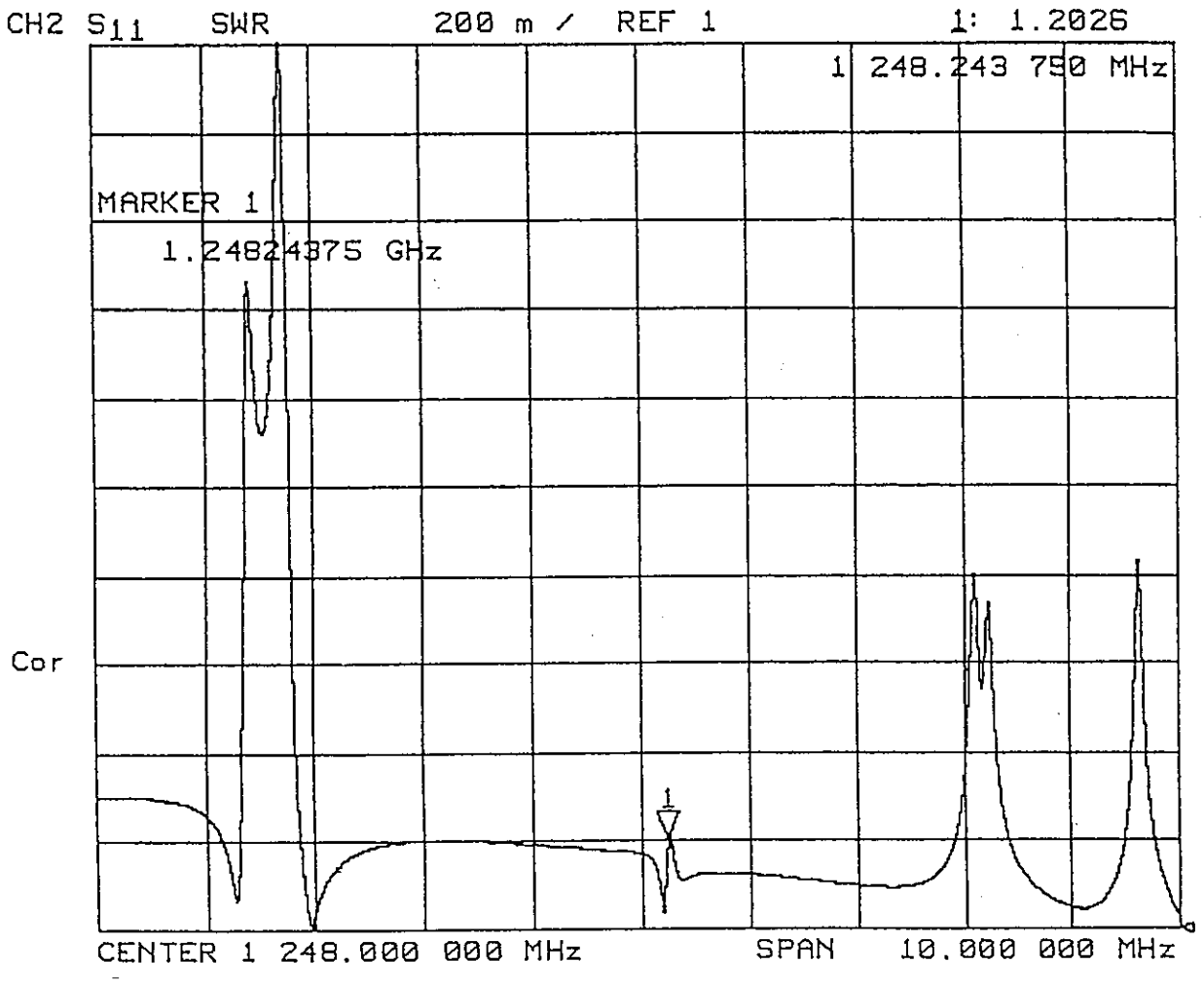

Fig.24, VSWR vs. f measured after tuning and matching for TWRR with the accelerator section

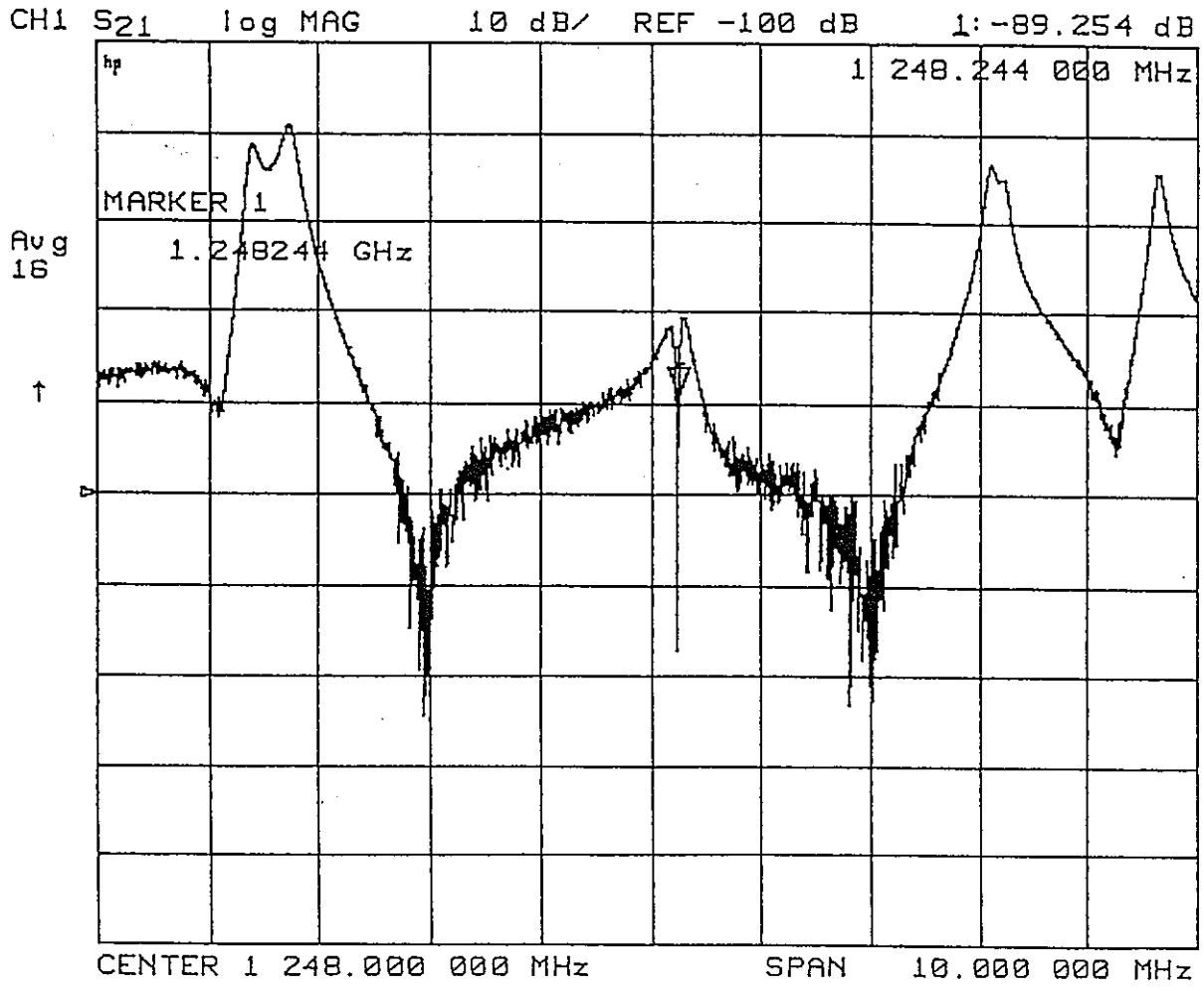

Fig.25, P3b vs. f measured after tuning and matching for TWRR with the accelerator section

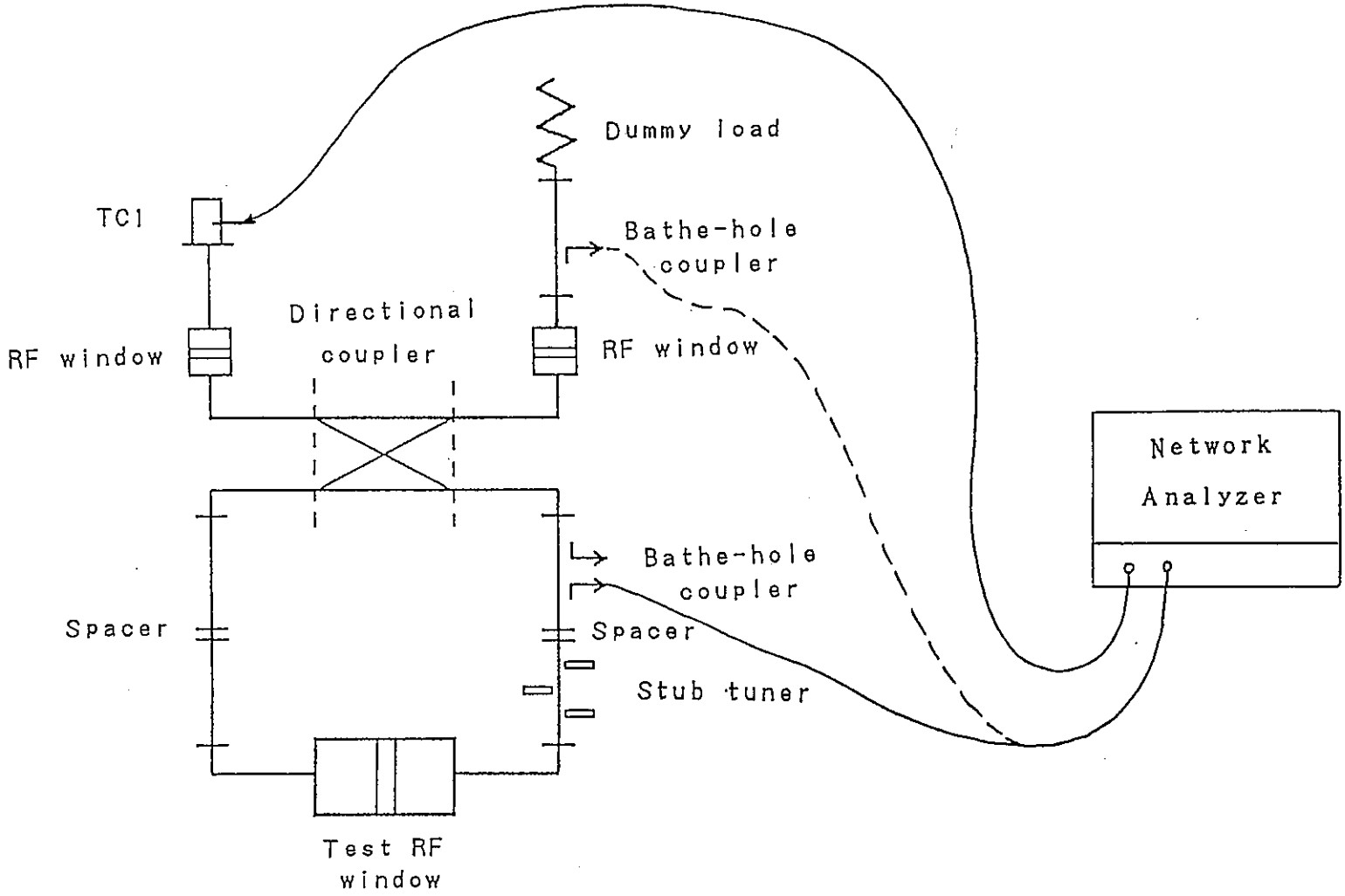

Fig.26, The low power test system for TWRR with the test RF window

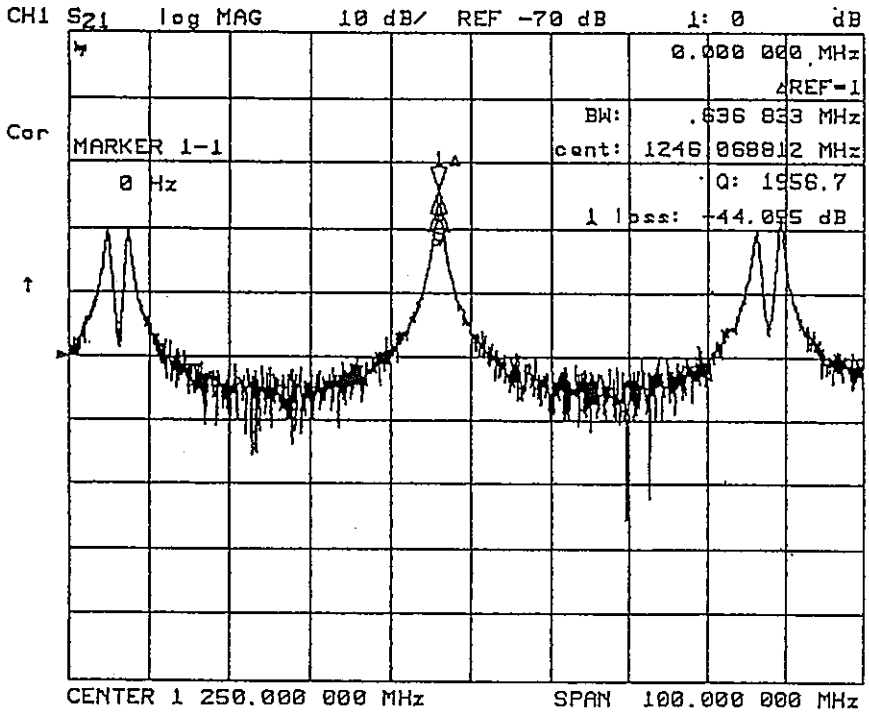

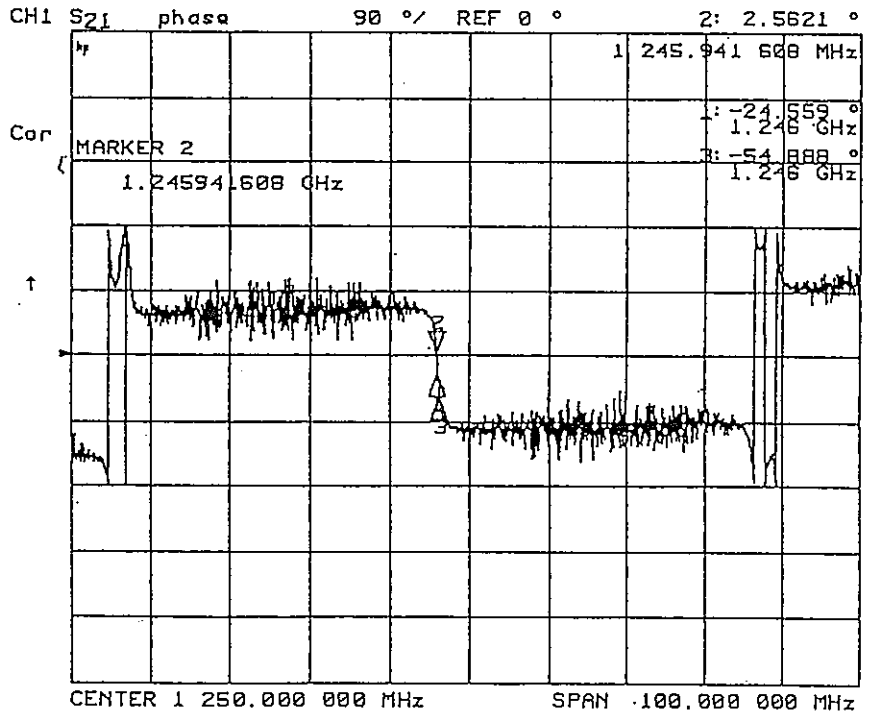

Fig.27, P3f vs. f and θ vs. f measured data for TWRR with the test RF window

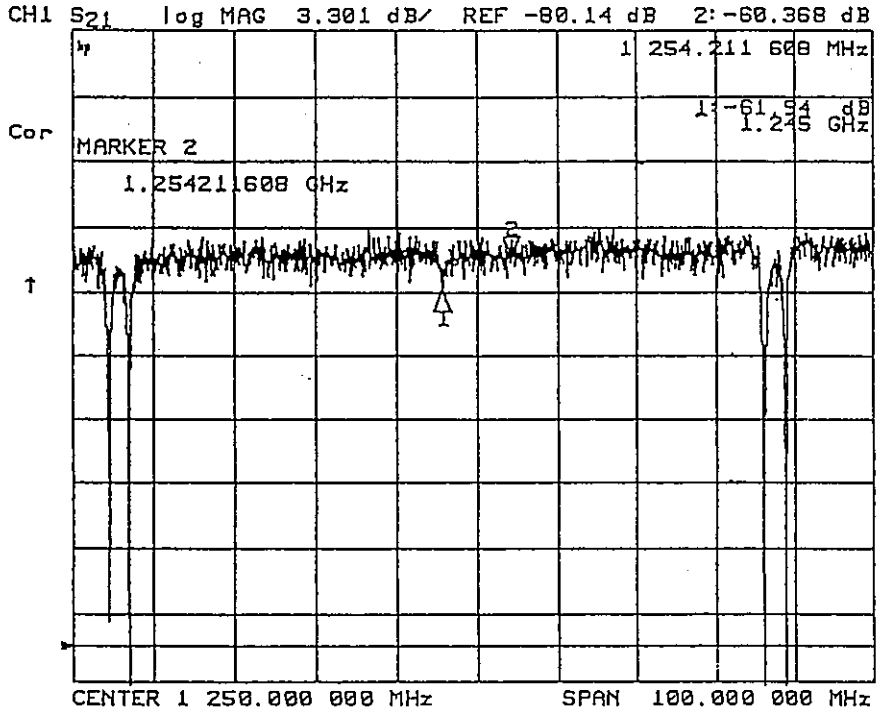

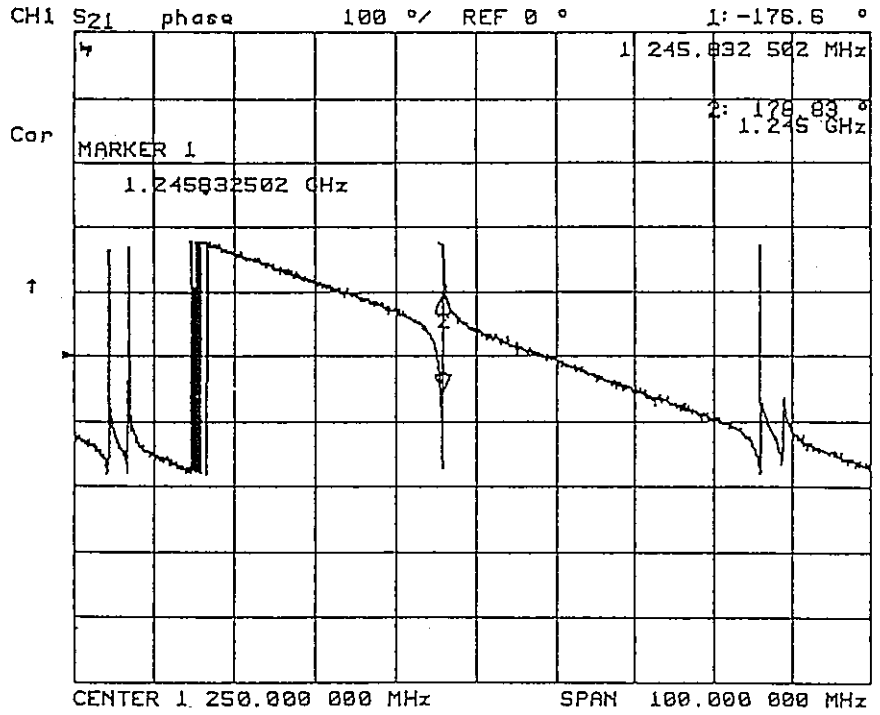

Fig.28, P4f vs. f and Ψ vs. f measured data for TWRR with the test RF window

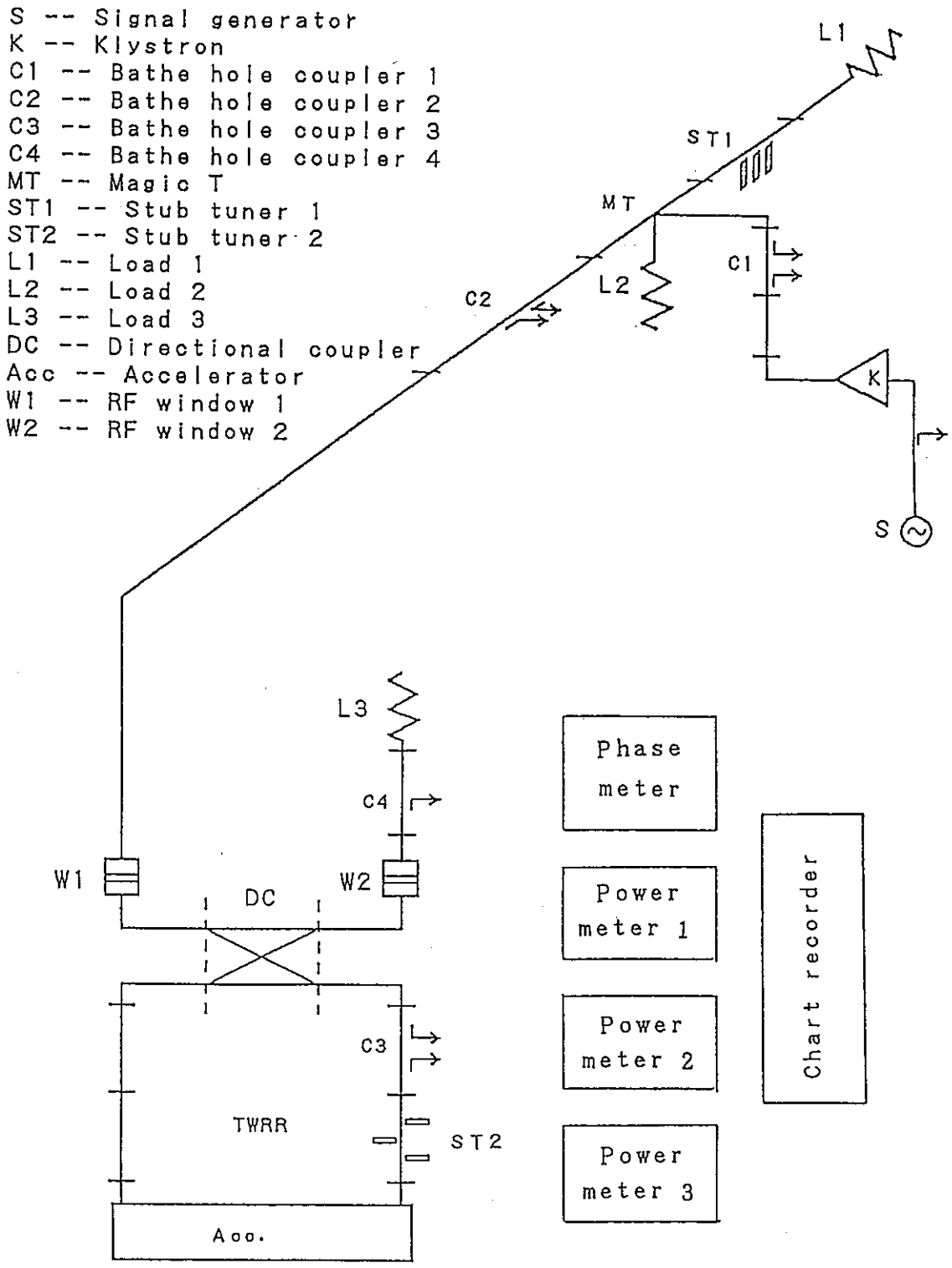

Fig.29, The high power test system for TWRR with the accelerator section

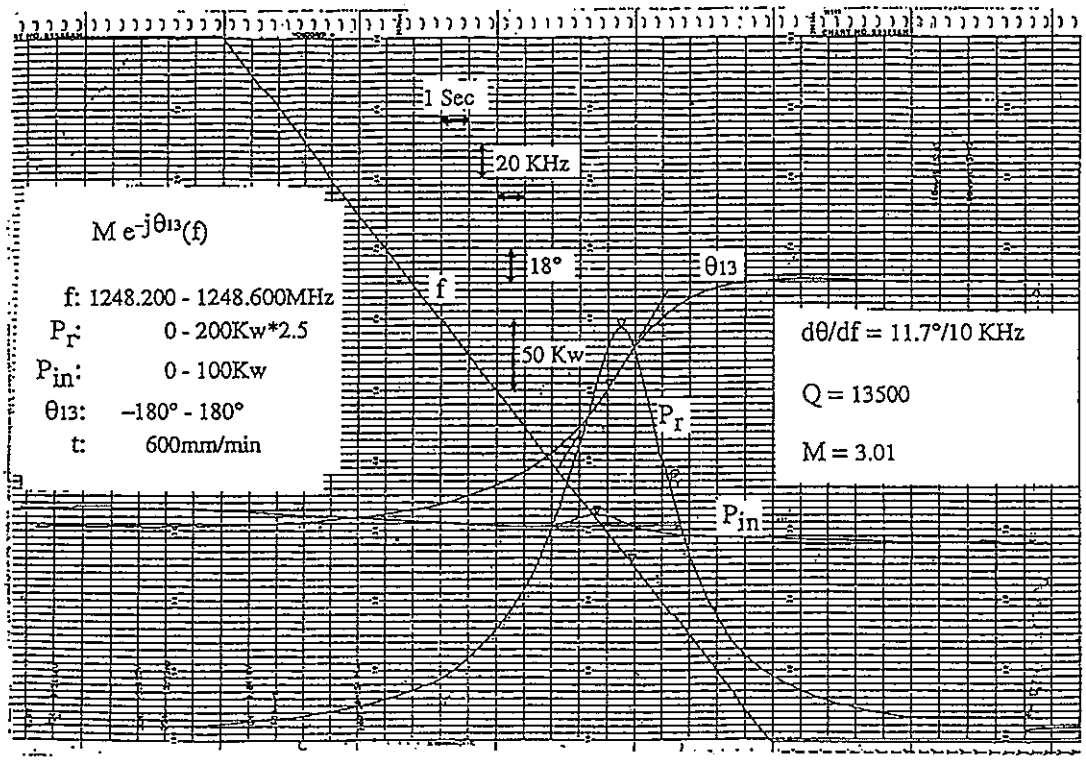

(a), frequency changing from low to high

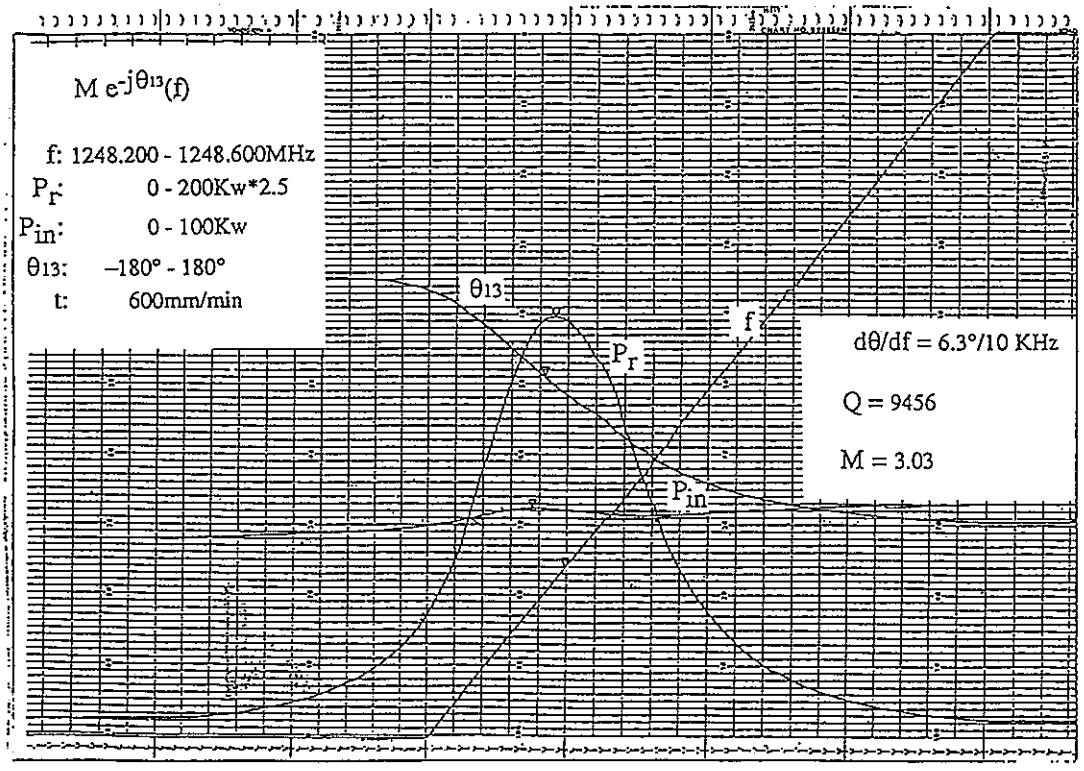

(b), frequency changing from high to low

Fig.30, M vs. f and θ vs. f by high power measured for TWRR with the accelerator section

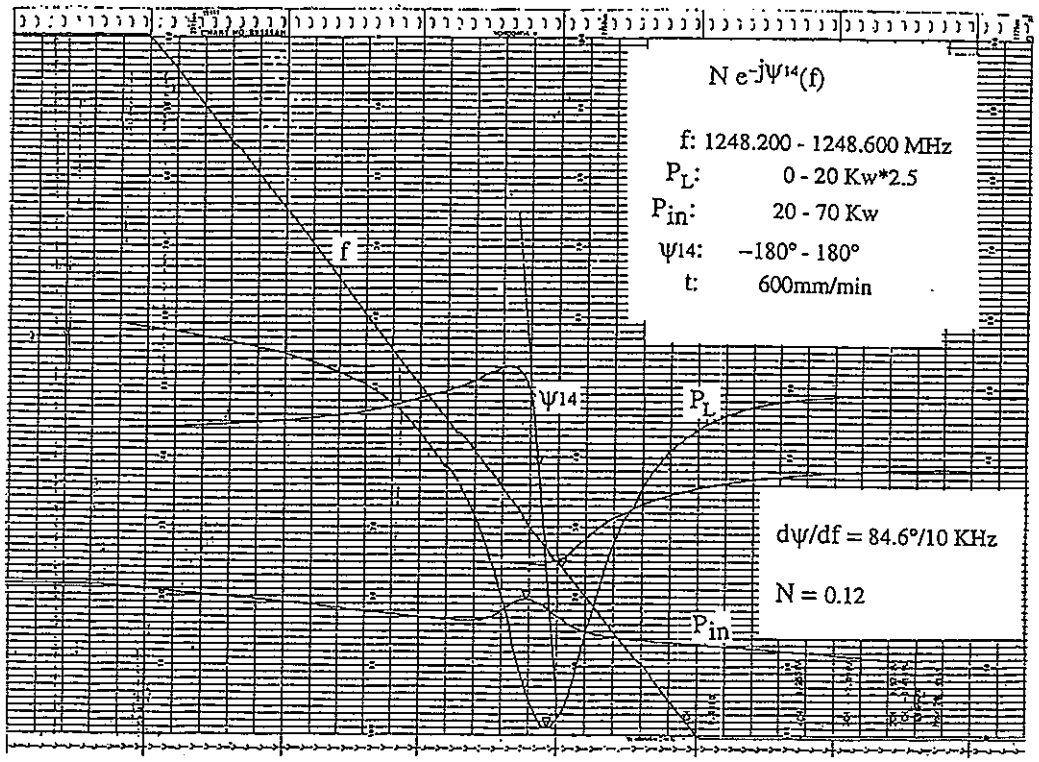

(a), frequency changing from low to high

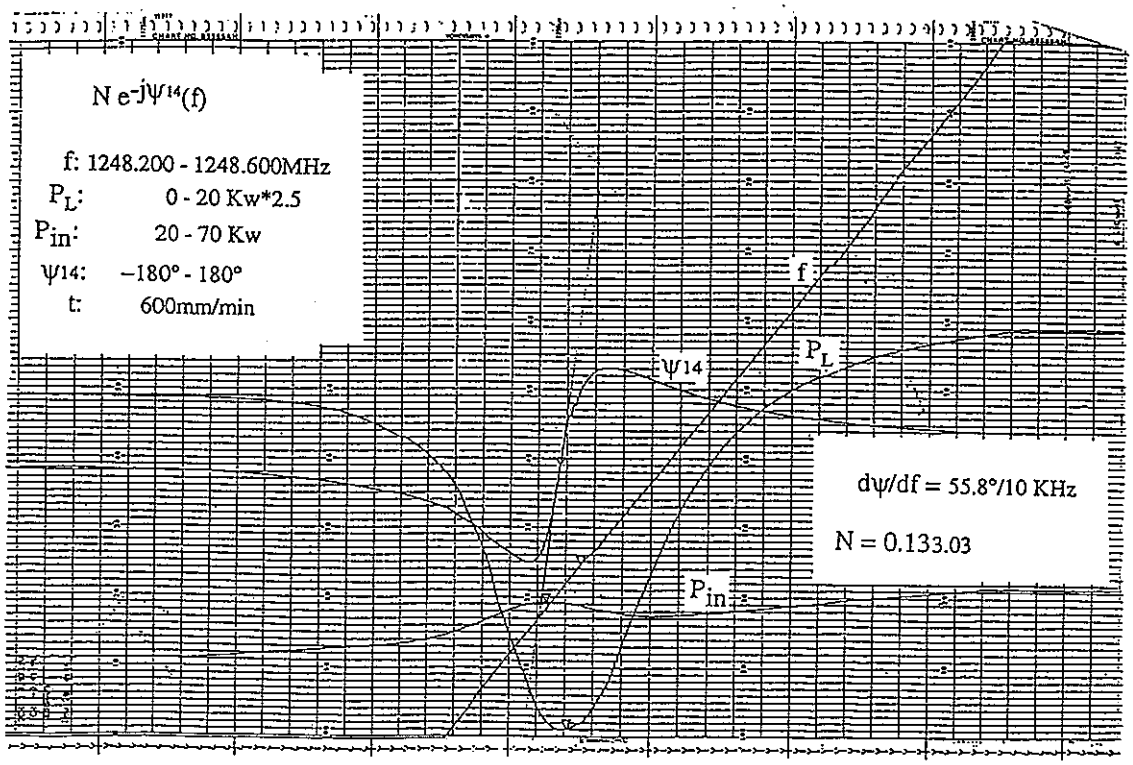

(b), frequency changing from high to low

Fig.31, N vs. f and ψ vs. f by high power measured for TWRR with the accelerator section

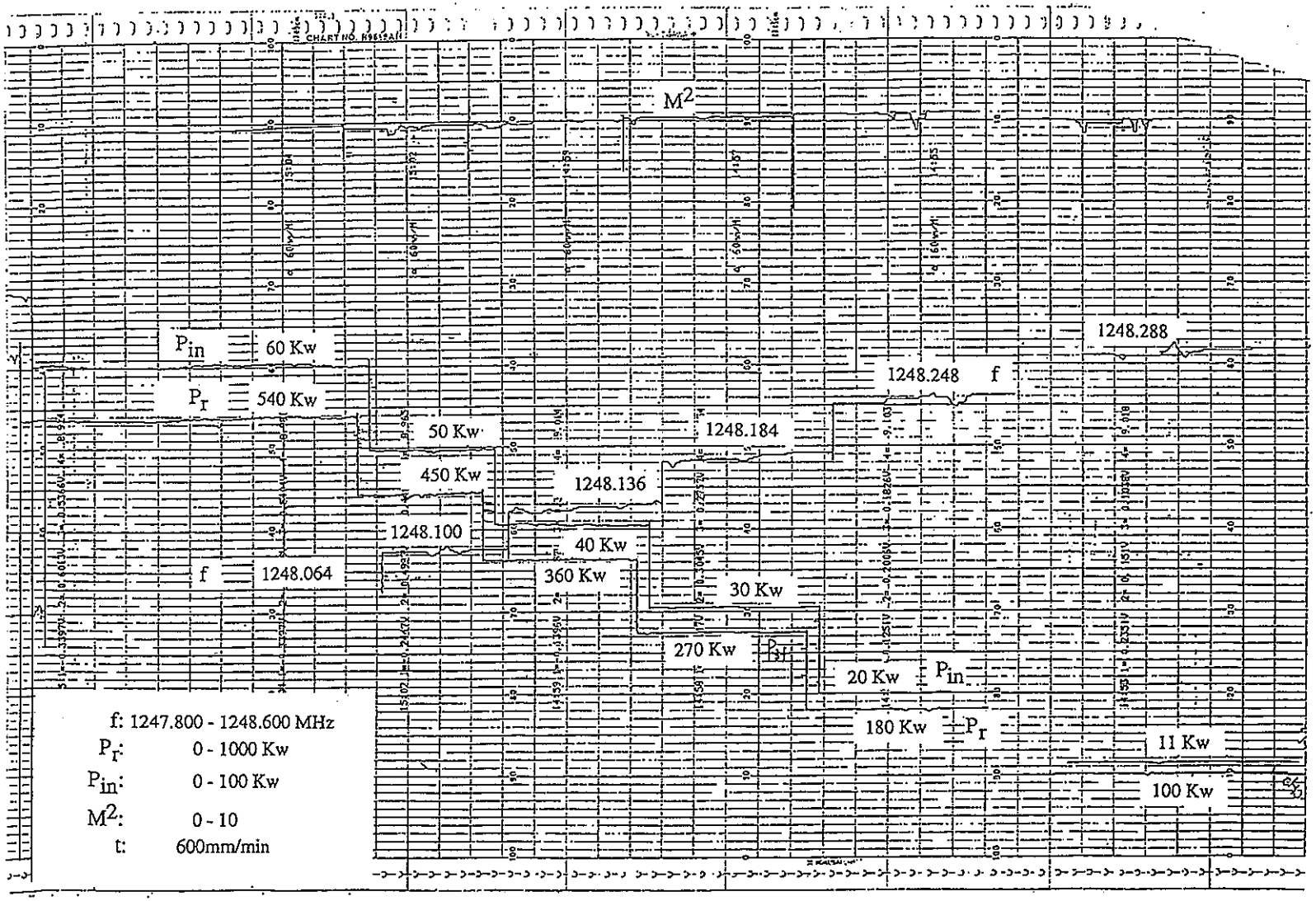

Fig.32, M vs. Pin by high power measured
for TWRR with the accelerator section

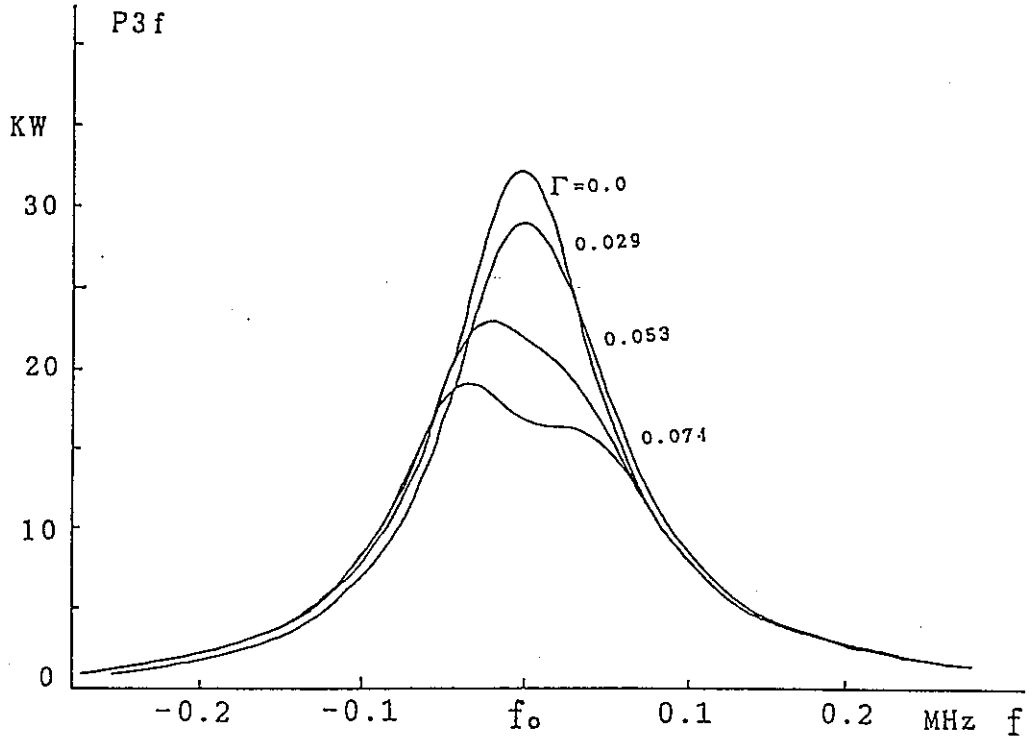

(a), P3f vs. f for different Γ

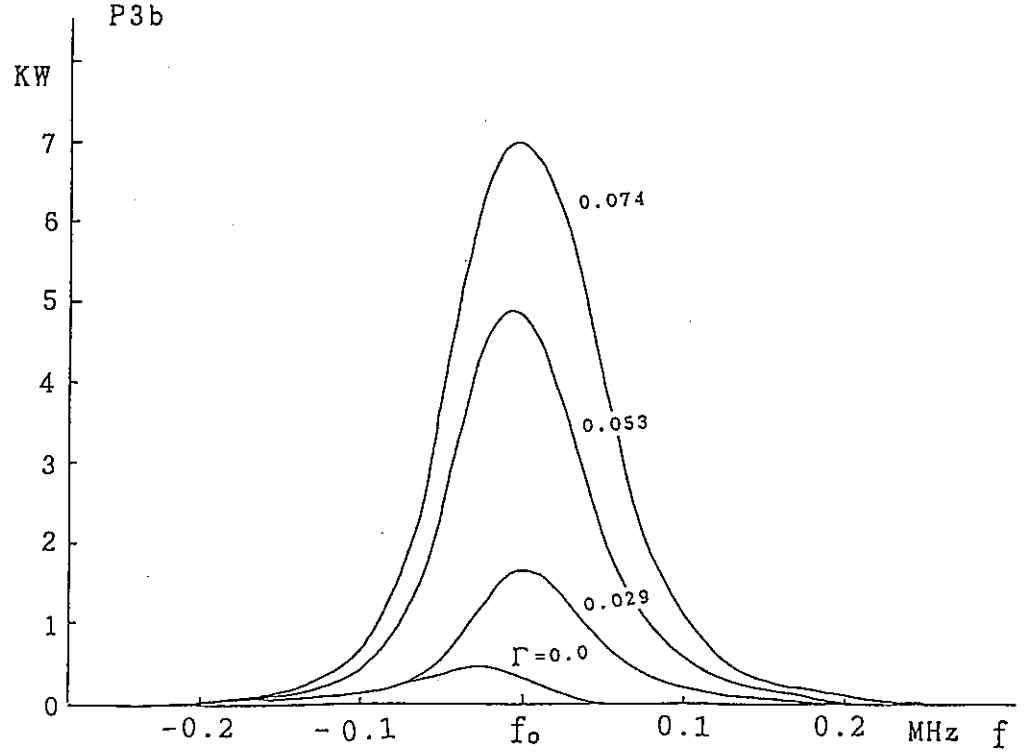

(b), P3b vs. f for different Γ

Fig.33, P3f vs. f and P3b vs. f for different for TWRR with the accelerator section

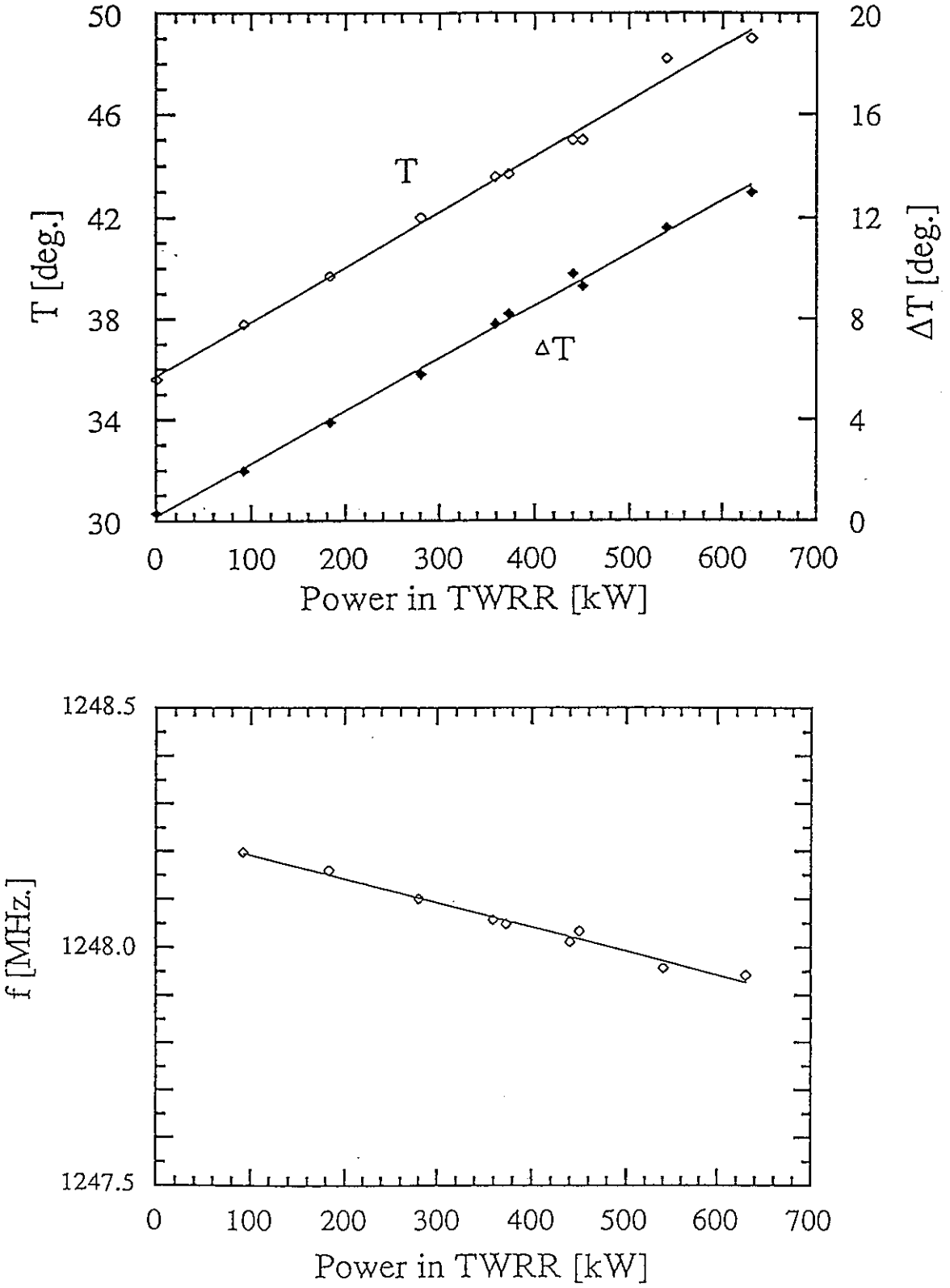

Fig.34, The thermal characteristics of the accelerator

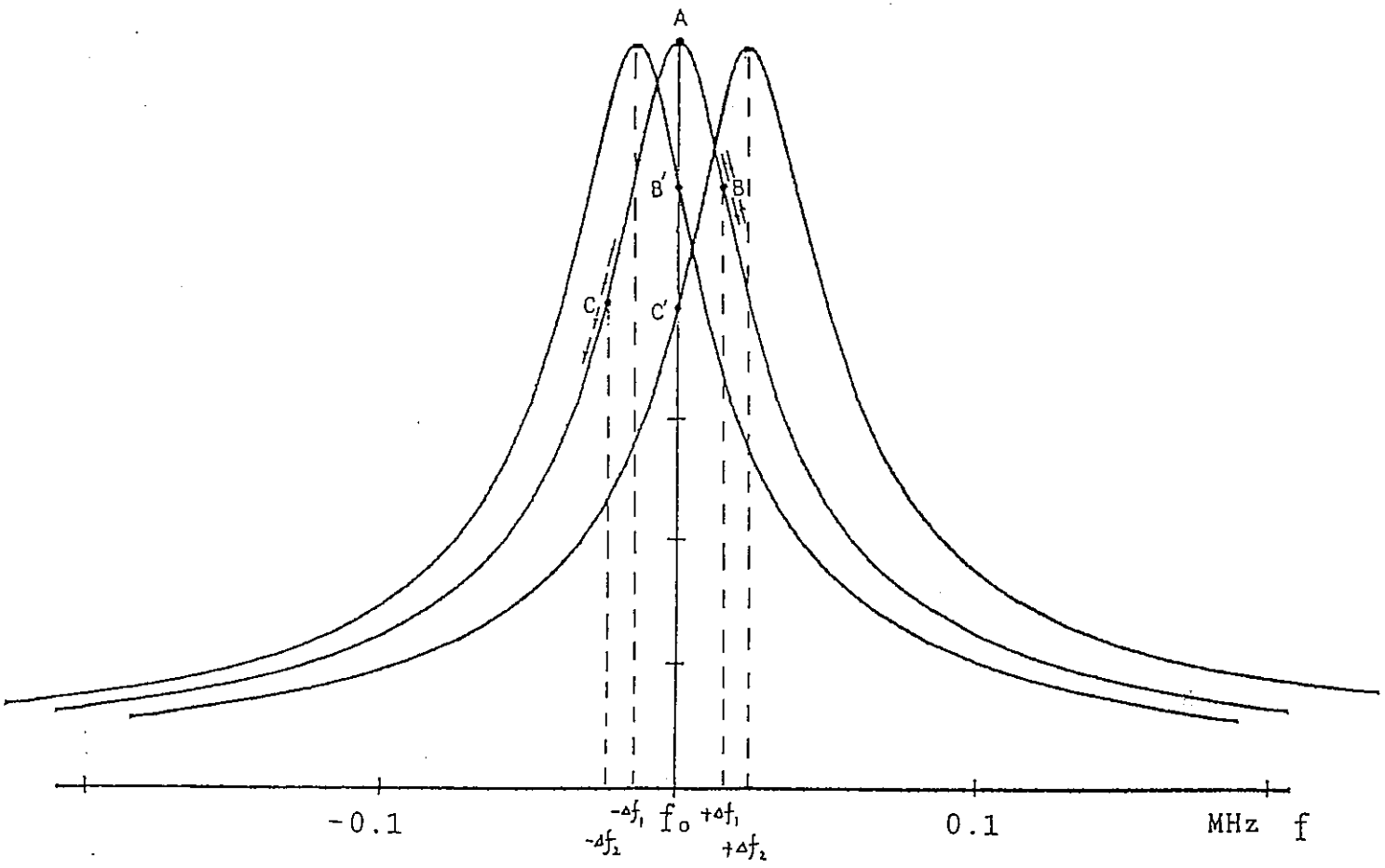

Fig.35, The resonant curve of TWRR

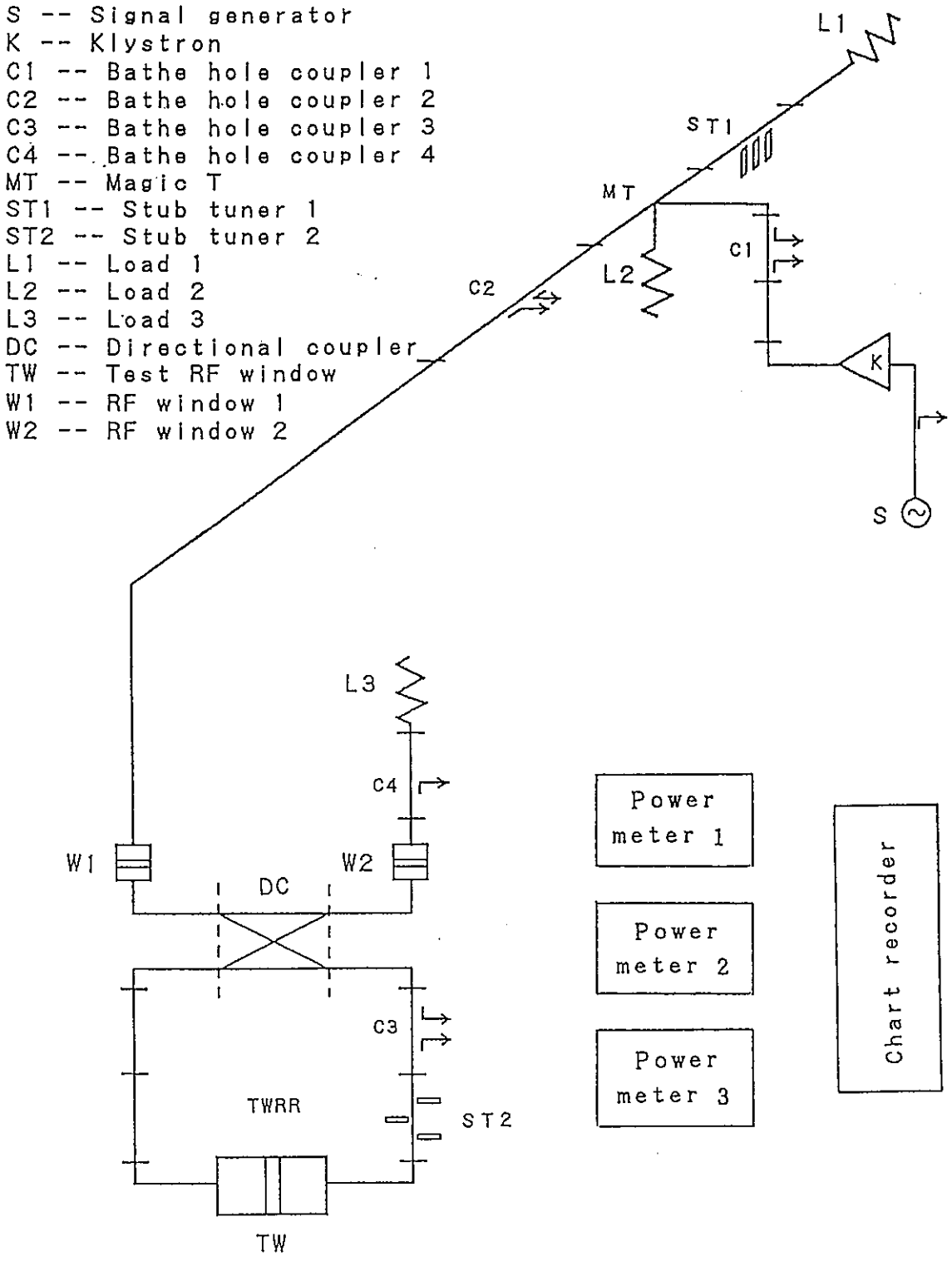

Fig.36, The high power test system for TWRR with the test RF window

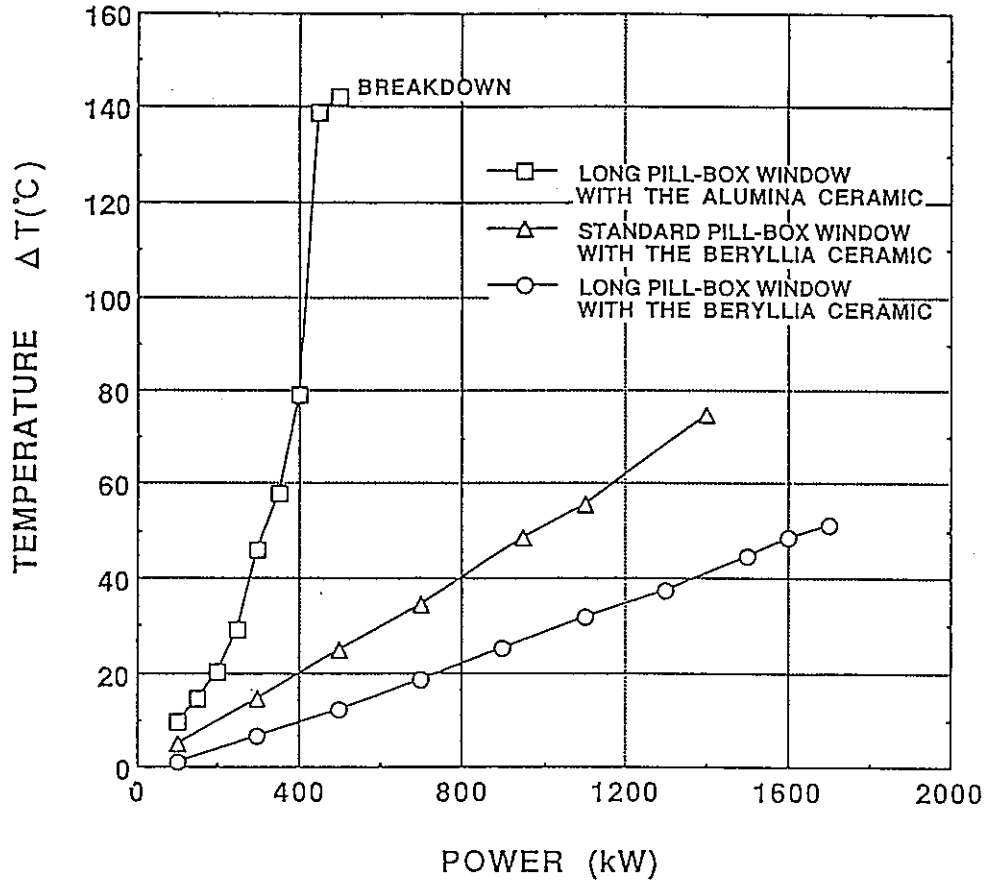

Fig.37, The thermal characteristic of the test RF window